Dalton Transactions

Accepted Manuscript

ROYAL SOCIETY OF CHEMISTRY

www.rsc.org/dalton

Catalytic Catechol Oxidation by Copper Complexes: Development of a Structure-Activity Relationship

Erica C.M. Ording-Wenker,[a] Maxime A. Siegler,[b] Martin Lutz,[c] and Elisabeth Bouwman*[a]

[a] Leiden Institute of Chemistry, Gorlaeus Laboratories, Leiden University, P.O. Box 9502, 2300 RA Leiden, The Netherlands, e-mail: bouwman@chem.leidenuniv.nl

[b] Department of Chemistry, Johns Hopkins University, Baltimore, Maryland 21218, United States

[c] Bijvoet Centre for Biomolecular Research, Utrecht University, Padualaan 8, 3584 CH Utrecht, The Netherlands

Abstract

A large library of Cu^{II} complexes with mononucleating and dinucleating ligands was synthesized to investigate their potential as catalysts for the catalytic oxidation of 3,5-di-tert-butylcatechol (3,5-DTBC). X-ray structure determination of a number of these complexes revealed relatively large Cu…Cu distances and the formation of polymeric species. Comparison of the 3,5-DTBC oxidation rates showed that ligands that stabilize the biomimetic dinuclear Cu^{II} μ-thiolate complex also result in copper compounds that are much more active in the oxidation of 3,5-DTBC. This oxidation activity is however inhibited by the presence of chloride ions. The highest k_{cat} that was observed was 6900 h^{-1}, which is one of the highest turnover frequencies reported so far for catechol oxidation in CH_3CN.

1. Introduction

The formation and redox properties of synthetic dinuclear Cu^{II} μ-thiolate complexes have been investigated because of their similarity to the Cu_A site.[1-6] It has been reported that small changes in the ligand structure can direct the reaction with copper salts towards the formation of either a Cu^{II} μ-thiolate or a Cu^{I} disulfide complex and that these species can interconvert (Figure 1a).[7, 8] Similar changes in the ligand structure can also induce a difference in coordination mode of dioxygen to copper.[9, 10] Additionally, the redox conversion of a $Cu^{II}_2(\mu\text{-}\eta^2\text{:}\eta^2\text{-peroxide})$ or a $Cu^{II}_2(\mu\text{-1,2-peroxide})$ complex into a $Cu^{III}_2(\mu\text{-oxide})_2$ species has been reported[11-13] suggesting that copper-oxygen chemistry might be very similar to copper-sulfur chemistry. To investigate this hypothesis we undertook a study of the biomimetic catalytic oxidation of 3,5-di-*tert*-butylcatechol (3,5-DTBC) to 3,5-di-*tert*-butyl-*o*-benzoquinone (3,5-DTBQ) using Cu^{II} complexes with mononucleating and dinucleating ligands containing sulfur donor atoms. The oxidation of catechol to quinone by catechol oxidase is assumed to proceed in two steps: the first molecule of catechol is oxidized by the binuclear Cu^{II} site with the formation of Cu^{I}_2 and two protons. In the second step the Cu^{I}_2 site reacts with O_2 to form a $Cu^{II}_2(\mu$-

η^2:η^2-peroxide) species, which oxidizes a second molecule of catechol with the formation of two molecules of water.[14-16] However, it has also been suggested that only one equivalent of catechol may be oxidized with the formation of dihydrogen peroxide, which would proceed via the $Cu^{II}_2(\mu$-η^2:η^2-peroxide) species.[17] This $Cu^{II}_2(\mu$-η^2:η^2-peroxide) species shows quite some similarities to the Cu^{II} μ-thiolate complex (Figure 1). Nevertheless, the involvement of other types of copper-oxygen intermediates cannot be ruled out.[18] The oxidation of 3,5-DTBC is easy to monitor and is used as a common test reaction for new biomimetic copper complexes.[16] The structural and electronic similarity between the Cu^{II} μ-thiolate and $Cu^{II}_2(\mu$-η^2:η^2-peroxide) complex might lead to a more effective or more stabilizing reaction with O_2 by complexes of ligands that promote Cu^{II} μ-thiolate formation. However, it is clear that if a Cu^{II} μ-thiolate species would form, it will be oxygenated by dioxygen.[19]

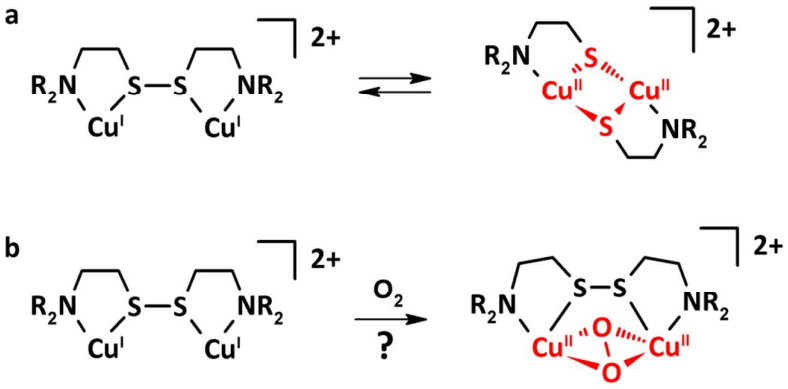

Figure 1: Schematic representation of (a) the equilibrium between a Cu^{I} disulfide and Cu^{II} μ-thiolate species and (b) the hypothesized reaction of a Cu^{I} disulfide complex with O_2 to form a side-on $Cu^{II}_2(\mu$-η^2:η^2-peroxide) species.

In this paper the synthesis of a series of Cu^{II} complexes with mononucleating and dinucleating ligands is described. To have a complete picture of the effect of small ligand changes on the catechol oxidation activity, a large library of ligands was rationally selected for this study (Figure 2). X-ray crystal structures were obtained for a number of copper complexes and some of these are discussed.

2. Results

2.1 Ligand and Complex Synthesis

Most of the ligands shown in Figure 2 were synthesized according to literature procedures or are commercially available.[4, 7, 8, 20-24] As the ligands are similar to each other, they were systematically named by their structure. For example **L**$^{\mathbf{1}}$ stands for the fragment *N,N*-bis(2-pyridylmethyl)aminoethyl and **Py** for 2-pyridylmethyl.

Ligand **L**$^{\mathbf{1}}$**SCH**$_{\mathbf{3}}$ was synthesized by reductive amination of 2-(methylthio)ethylamine, avoiding the use of toxic 2-chloroethyl methyl sulfide,[25] and increasing the yield from 53% to 99%. A similar

synthesis was used for the formation of **L^1OH** increasing the reported yield from 85% to 99%.[26] The ligand **Py_2S** has been reported, but its synthesis has not been described elaborately.[27] Four new ligands were designed: **L^1SL^1**, **L^1*SCH_3**, **L^2SCH_3** and **L^3SCH_3**. **L^1SL^1** was synthesized by reductive amination of 1,5-diamino-3-thiapentane dihydrobromide, which was made via a 4-step literature procedure.[28] **L^1SL^1** was obtained in 68% yield as brown oil. **L^1*SCH_3** was synthesized by reaction of propylene sulfide with di-(2-pyridylmethyl)amine in acetonitrile. After solvent evaporation, tetrahydrofuran and NaH were added to deprotonate the thiol. Addition of CH_3I yields **L^1*SCH_3**, which was purified by column chromatography, resulting in 86% yield. **L^2SCH_3** and **L^3SCH_3** were obtained in relatively moderate yields of 50% and 46% by a two-step reductive amination using $NaBH_4$. All synthesized ligands degrade over a period of weeks, even when stored under argon at 0 °C, as indicated by darkening of the oil. When the ligands are coordinated to copper, the complexes do are stable over time. A schematic overview of the syntheses of the new ligands is shown in the Supporting Information.

With the 22 ligands, Cu^{II} complexes were formed with one Cl^- and one BF_4^- counterion per copper center. The general synthesis of these complexes entails the addition of a 1:1 mixture of $[Cu^{II}(H_2O)_6](BF_4)_2$ and $Cu^{II}Cl_2 \cdot 2\ H_2O$ to the ligand dissolved in methanol, or in the case of **L^2SSL^2** and **L^1NH_2** in CH_3CN. If the complex did not precipitate spontaneously, precipitation was induced by addition of diethyl ether. Copper compounds of ligands that can potentially form dinuclear complexes are more likely to form polymeric structures (see Section 2.2), and are tentatively indicated with the formula $[Cu^{II}_2(\text{ligand})(Cl)_2]_n(BF_2)_n$. The complexes of ligands that are expected to form mononuclear compounds are indicated with the formula $[Cu^{II}(\text{ligand})(Cl)](BF_4)$. A copper complex with **L^5SSL^5** could not be isolated as a solid; all attempts resulted in the formation of oil. For the catalytic experiments, this complex was formed in situ. In the synthesis of a complex with **L^2SSL^2**, $[Cu^{II}(H_2O)_6](ClO_4)_2$ was used instead of $[Cu^{II}(H_2O)_6](BF_4)_2$ to grow single crystals suitable for X-ray structure diffraction. However, the complex $[Cu^{II}_2(\mathbf{L^2SSL^2})(Cl)_2]_n(BF_4)_{2n}$ was also synthesized, so that all catalysts used for catechol oxidation have the same counterions. With the ligand **L^1*SCH_3** two complexes were formed: $[Cu^{II}(\mathbf{L^1}$*$\mathbf{SCH_3})(Cl)]_2(CuCl_4)$ and $[Cu^{II}(\mathbf{L^1}$*$\mathbf{SCH_3})(Cl)](BF_4)$. The first compound was obtained by addition of 1 equiv of $Cu^{II}Cl_2 \cdot 2\ H_2O$ to **L^1*SCH_3**, the latter from 0.5 equiv of $Cu^{II}Cl_2 \cdot 2\ H_2O$ and 0.5 equiv. of $[Cu^{II}(H_2O)_6](BF_4)_2$. The X-ray crystal structures were determined for both complexes and the structures of their cationic copper complex were found to be very similar. The Supporting Information contains the crystallographic information for both structures.

The UV-vis spectra of all the Cu^{II} complexes are highly similar, showing LMCT bands of $Cu^{II} \leftarrow S$ and $Cu^{II} \leftarrow Cl$ in the region between 200 and 400 nm and one or two bands in the range of 650 to 940 nm that can be ascribed to Cu^{II} d-d transitions (Figure S7).

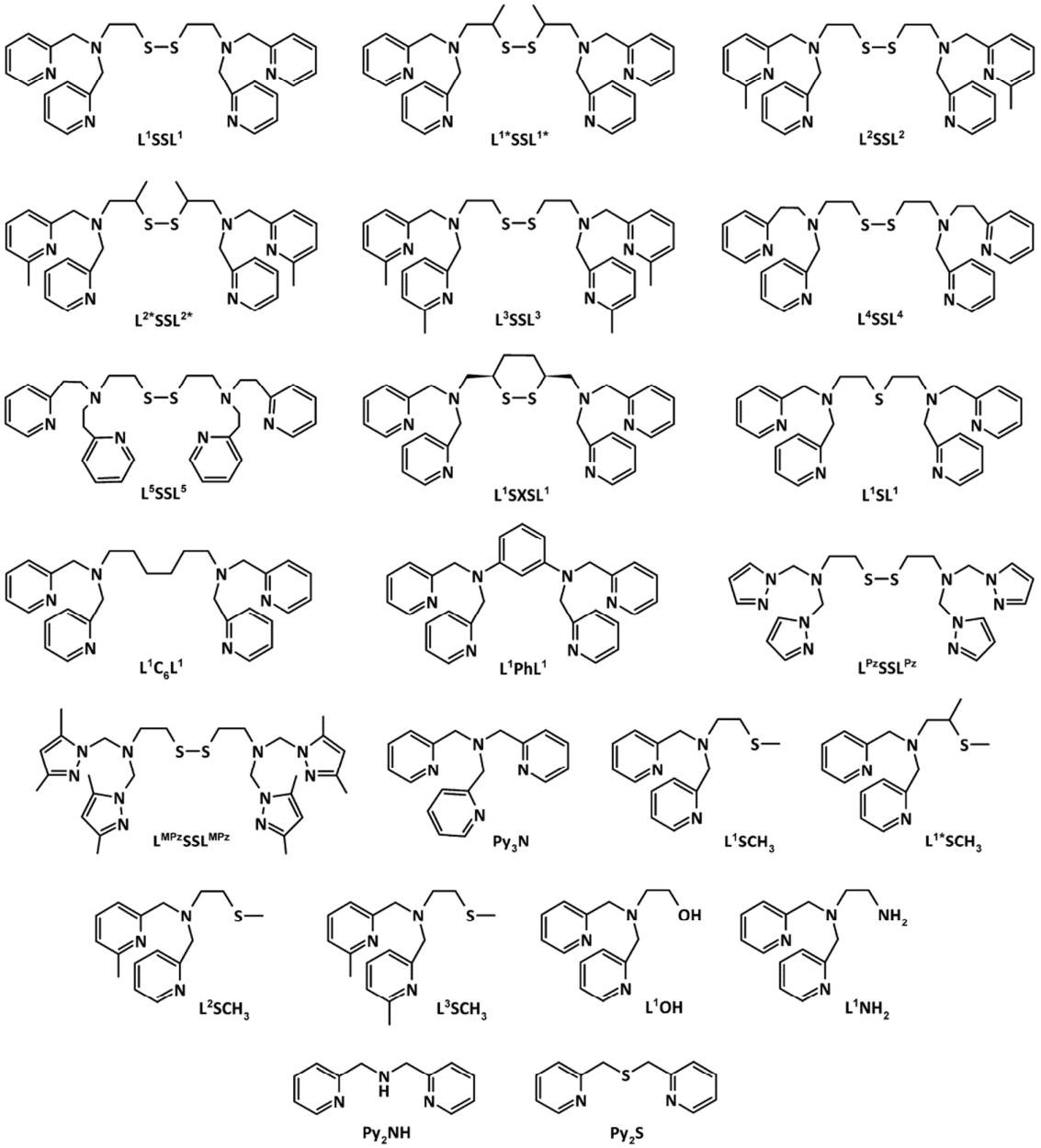

Figure 2: Schematic overview of the ligands that were synthesized for the study of the copper-catalyzed oxidation of catechol.

2.2 Single Crystal X-ray Crystallography

Single crystals could be obtained for several of the synthesized Cu^{II} complexes. This led to the X-ray crystal structure determination of the polymeric complexes $[Cu^{II}_2(\mathbf{L^1SSL^1})(Cl)_2]_n(BF_4)_{2n}$, $[Cu^{II}_2(\mathbf{L^2SSL^2})(Cl)_2]_n(ClO_4)_{2n}$, $[Cu^{II}_2(\mathbf{L^1SL^1})(Cl)_2]_n(BF_4)_{2n}$ and $[Cu^{II}_2(\mathbf{L^1C_6L^1})(Cl)_2]_n(BF_4)_{2n}$ and of the compounds of mononucleating ligands, namely $[Cu^{II}(\mathbf{L^1SCH_3})(Cl)](BF_4)$, $[Cu^{II}(\mathbf{L^1*SCH_3})(Cl)](BF_4)$, $[Cu^{II}(\mathbf{L^1*SCH_3})(Cl)]_2(CuCl_4)$, $[Cu^{II}(\mathbf{L^2SCH_3})(Cl)](BF_4)$, $[Cu^{II}(\mathbf{L^3SCH_3})(Cl)](BF_4)$ and $[Cu^{II}(\mathbf{L^1NH_2})(Cl)](BF_4)$. The copper ions in the polymeric structures $[Cu^{II}_2(\mathbf{L^1SSL^1})(Cl)_2]_n(BF_4)_{2n}$,

$[Cu^{II}_2(\mathbf{L^2SSL^2})(Cl)_2]_n(ClO_4)_{2n}$ and $[Cu^{II}_2(\mathbf{L^1SL^1})(Cl)_2]_n(BF_4)_{2n}$ have very similar coordination geometries; $[Cu^{II}_2(\mathbf{L^1SSL^1})(Cl)_2]_n(BF_4)_{2n}$ and $[Cu^{II}_2(\mathbf{L^2SSL^2})(Cl)_2]_n(ClO_4)_{2n}$ will not be discussed, but crystallographic data and selected bond distances and angles can be found in the Supporting Information. Similarly, the structures of $[Cu^{II}(\mathbf{L^1{*}SCH_3})(Cl)](BF_4)$, $[Cu^{II}(\mathbf{L^1{*}SCH_3})(Cl)]_2(CuCl_4)$ and $[Cu^{II}(\mathbf{L^2SCH_3})(Cl)](BF_4)$ are comparable to that of $[Cu^{II}(\mathbf{L^1SCH_3})(Cl)](BF_4)$ and detailed information concerning these structures can be found in the Supporting Information. Thus, the structures of $[Cu^{II}_2(\mathbf{L^1SL^1})(Cl)_2]_n(BF_4)_{2n}$, $[Cu^{II}_2(\mathbf{L^1C_6L^1})(Cl)_2]_n(BF_4)_{2n}$, $[Cu^{II}(\mathbf{L^1SCH_3})(Cl)](BF_4)$, $[Cu^{II}(\mathbf{L^3SCH_3})(Cl)](BF_4)$, and $[Cu^{II}(\mathbf{L^1NH_2})(Cl)](BF_4)$ are described. The crystallographic and structure refinement data for these complexes are collected in Table 1.

Table 1: Crystallographic and structure refinement data for $[Cu^{II}_2(\mathbf{L^1SL^1})(Cl)_2]_n(BF_4)_{2n}$, $[Cu^{II}_2(\mathbf{L^1C_6L^1})(Cl)_2]_n(BF_4)_{2n}$, $[Cu^{II}(\mathbf{L^1SCH_3})(Cl)](BF_4)$, $[Cu^{II}(\mathbf{L^3SCH_3})(Cl)](BF_4)$ and $[Cu^{II}(\mathbf{L^1NH_2})(Cl)](BF_4)$.

	$[Cu^{II}_2(\mathbf{L^1SL^1})(Cl)_2]_n(BF_4)_{2n}$	$[Cu^{II}_2(\mathbf{L^1C_6L^1})(Cl)_2]_n(BF_4)_{2n}$	$[Cu^{II}(\mathbf{L^1SCH_3})(Cl)](BF_4)$	$[Cu^{II}(\mathbf{L^3SCH_3})(Cl)](BF_4)$	$[Cu^{II}(\mathbf{L^1NH_2})(Cl)](BF_4)$
empirical formula	$[C_{28}H_{32}Cl_2Cu_2N_6S](BF_4)_2$	$[C_{30}H_{36}Cl_2Cu_2N_6](BF_4)_2 \cdot 4\,CH_3CN$	$[C_{15}H_{19}ClCuN_3S](BF_4)$	$[C_{17}H_{23}ClCuN_3S](BF_4)$	$[C_{14}H_{18}ClCuN_4](BF_4)$
formula weight	856.25	1016.46	459.19	487.24	428.12
crystal system	monoclinic	monoclinic	triclinic	monoclinic	monoclinic
space group	*C*2/*c*	*C*2/*m*	*P*–1	*P*2$_1$/c	*P*2$_1$/*n*
a, Å	10.0603(8)	13.287(2)	7.45273(18)	9.11412(10)	8.92176(15)
b, Å	23.2653(15)	27.558(5)	11.2448(3)	15.17627(13)	12.8949(3)
c, Å	14.5686(9)	6.9232(17)	12.3634(3)	15.31060(15)	14.9606(3)
α, deg	90	90	65.993(3)	90	90
β, deg	100.321(7)	111.421(13)	74.934(2)	102.6105(10)	102.0565(19)
γ, deg	90	90	88.273(2)	90	90
V, Å^3	3354.7(4)	2359.9(8)	910.58(4)	2066.65(4)	1683.18(6)
Z	4	2	2	4	4
D_{calc}, g·cm^3	1.695	1.430	1.675	1.566	1.689
T, Kelvin	110(2)	150(2)	110(2)	110(2)	110(2)
crystal size, mm	0.43×0.14×0.08	0.30×0.30×0.30	0.36×0.28×0.22	0.40×0.32×0.22	0.50×0.36×0.14
μ, mm^{-1}	1.566	1.085	1.504	4.021	1.502
no. of reflns measd	9412	9970	28025	14162	13962
no. of unique reflns	2953	1904	4179	4035	3879
no. of reflns obsd. [$I > 2\sigma(I)$]	2550	1601	3994	3893	3414
no. of parameters	444	172	282	303	234
R_1 / wR_2 [$I > 2\sigma(I)$]	0.0538/0.1394	0.0780/0.2007	0.0187/0.0486	0.0240/0.0635	0.0257/0.0675
R_1 / wR_2 [all refl.]	0.0621/0.1452	0.0942/0.2123	0.0197/0.0491	0.0250/0.0641	0.0305/0.0693
goodness of fit	1.029	1.151	1.043	1.054	1.080
$\Delta\rho$, e·Å^{-3}	−0.57/0.81	−1.22/1.04	–0.30/0.36	−0.30/0.39	−0.48/0.31

Single crystals of $[Cu^{II}_2(\mathbf{L^1SL^1})(Cl)_2]_n(BF_4)_{2n}$ were obtained by slow evaporation of diethyl ether into a solution of the complex in acetonitrile. A displacement ellipsoid plot of $[Cu^{II}_2(\mathbf{L^1SL^1})(Cl)_2]_n(BF_4)_{2n}$ is

shown in Figure 3 and selected bond distances and angles are provided in Table 2. The structure of $[Cu^{II}_2(\mathbf{L^1SL^1})(Cl)_2]_n(BF_4)_{2n}$ is very disordered; both the Cu complex and the BF_4^- counterions are disordered over two orientations. The major and minor components of the Cu complex are related by a pseudo-mirror plane; the occupancy factor of the major component of the disorder refines to 0.840(3). Both counterions are found at sites of twofold axial symmetry, and are thus constrained to be disordered with an occupancy factor of 0.5. The thioether sulfur atom of the dinucleating ligand bridges between the two copper ions, resulting in a distorted octahedral N_3SCl_2 coordination environment for both copper ions. The elongated Jahn-Teller axis is occupied by S1 and Cl1* (Cu1-S1 2.6825(7) Å; Cu1-Cl1* 2.879(2) Å). The chloride ions are bridging between copper ions of neighboring dinuclear complexes resulting in infinite 1D zig-zag chains. The distance between the copper ions in the Cu(μ-Cl)$_2$Cu core is 3.6986(7) Å. This distance is slightly larger than the Cu…Cu distances in $[Cu^{II}_2(\mathbf{L^1SSL^1})(Cl)_2]_n(BF_4)_{2n}$ and $[Cu^{II}_2(\mathbf{L^2SSL^2})(Cl)_2]_n(BF_4)_{2n}$, which are *ca.* 3.60 Å (average) and 3.6455(4) Å, respectively (Table S2).

Table 2: Selected bond distances (Å) and bond angles (°) for $[Cu^{II}_2(\mathbf{L^1SL^1})(Cl)_2]_n(BF_4)_{2n}$ and $[Cu^{II}_2(\mathbf{L^1C_6L^1})(Cl)_2]_n(BF_4)_{2n}$.

	$[Cu^{II}_2(\mathbf{L^1SL^1})(Cl)_2]_n(BF_4)_{2n}$	$[Cu^{II}_2(\mathbf{L^1C_6L^1})(Cl)_2]_n(BF_4)_{2n}$
Cu1 - Cu1*	3.6986(7)	3.405(2)
Cu1 - Cu1#	5.0511(7)	12.013(3)
Cu1 - S1	2.6825(7)	
Cu1 - N1	2.057(4)	2.026(9)
Cu1 - N11/N2	2.004(4)	1.987(6)
Cu1 - N21/N2’	1.987(4)	1.987(6)
Cu1 - Cl1	2.278(2)	2.223(3)
Cu1 - Cl1*	2.879(2)	2.865(4)
S1 - Cu1 - N1	84.72(12)	
S1 - Cu1 - N11	83.29(11)	
S1 - Cu1 - N21	100.27(11)	
S1 - Cu1 - Cl1*	166.13(5)	
N1 - Cu1 - N11/N2	82.77(18)	82.88(18)
N1 - Cu1 - N21/N2’	80.87(17)	82.88(18)
N1 - Cu1 - Cl1	177.93(13)	173.7(3)
N11 - Cu1 - N21/N2’	162.84(18)	165.5(4)

Symmetry operation * = [1–x, –y, –z] and # = [1–x, y, ½–z] for $[Cu^{II}_2(\mathbf{L^1SL^1})(Cl)_2]_n(BF_4)_{2n}$; Symmetry operation * = [1–x, y, 1–z]; # = [–x, y, –1–z]; ‘ = [x, –y, z] for $[Cu^{II}_2(\mathbf{L^1C_6L^1})(Cl)_2]_n(BF_4)_{2n}$.

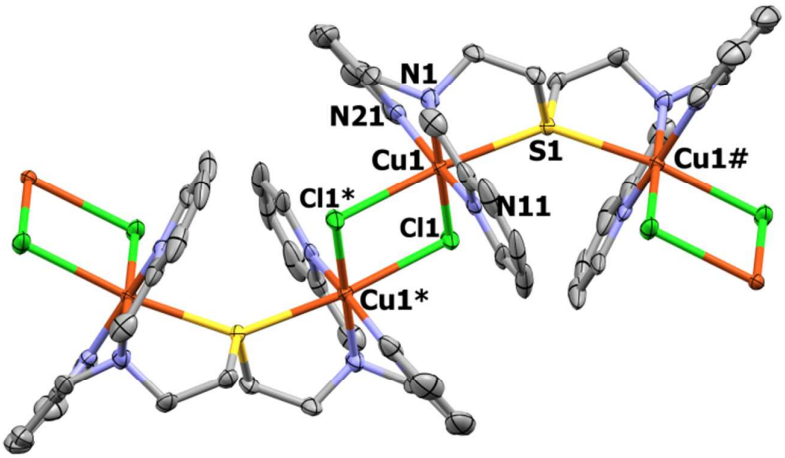

Figure 3: Displacement ellipsoid plot (50% probability level) of two of the repeating units in the cationic polymer chain of $[Cu^{II}_2(\mathbf{L^1SL^1})(Cl)_2]_n(BF_4)_{2n}$. The disorder, the non-coordinating counterions and hydrogen atoms are omitted for clarity. Symmetry operation * = [1–x, –y, –z] and # = [1–x, y, ½–z].

$[Cu^{II}_2(\mathbf{L^1C_6L^1})(Cl)_2]_n(BF_4)_{2n} \cdot 4\ CH_3CN$ crystallized from acetonitrile and di-isopropyl ether. The metal and chloride ions and the 1,6-diaminohexane backbone are lying in a mirror plane and in addition the molecule contains two-fold rotational symmetry; the BF_4^- anion is disordered on a twofold axis, and the acetonitrile molecule is located on a general position. The asymmetric unit consequently contains ¼ of the ligand, half a copper center, half a Cl^- ion, half a BF_4^- ion and one CH_3CN molecule. A displacement ellipsoid plot is shown in Figure 4, selected bond distances and angles can be found in Table 2. The copper ions in $[Cu^{II}_2(\mathbf{L^1C_6L^1})(Cl)_2]_n(BF_4)_{2n}$ are in an N_3Cl_2 coordination environment, in a distorted square-pyramidal geometry that resembles that of the copper ions in $[Cu^{II}_2(\mathbf{L^1SL^1})(Cl)_2]_n(BF_4)_{2n}$, except for the coordination of a sulfur atom. The chloride ions are bridging between copper ions of neighboring dinuclear complexes resulting in infinite linear 1D chains. The Cu1-Cu1* distance in the Cu(μ-Cl)$_2$Cu core is 3.405(2) Å, which is significantly smaller than in sulfur-containing complexes such as $[Cu^{II}_2(\mathbf{L^1SL^1})(Cl)_2]_n(BF_4)_{2n}$. The structure of the related dinuclear complex $[Cu^{II}_2(\mathbf{L^1C_6L^1})(Cl)_4]$, which does not form polymeric structures, was recently reported;[29] the copper ions in the two structures have very similar coordination geometries (Figure S6). The major difference between the structures is that the hexamethylene bridge in $[Cu^{II}_2(\mathbf{L^1C_6L^1})(Cl)_4]$ has a crystallographic C_{2h} symmetry and forms an 'alternating' chain whereas in $[Cu^{II}_2(\mathbf{L^1C_6L^1})(Cl)_2]_n(BF_4)_{2n}$ it forms a linear chain, which is the expected, thermodynamically favored conformation.

The three compounds $[Cu^{II}(\mathbf{L^1SCH_3})(Cl)](BF_4)$, $[Cu^{II}(\mathbf{L^3SCH_3})(Cl)](BF_4)$ and $[Cu^{II}(\mathbf{L^1NH_2})(Cl)](BF_4)$ all crystallized with one mononuclear complex cation and one BF_4^- counterion in the asymmetric unit. Displacement ellipsoid plots and selected bond distances and angles are given in Figure 5 and Table 3.

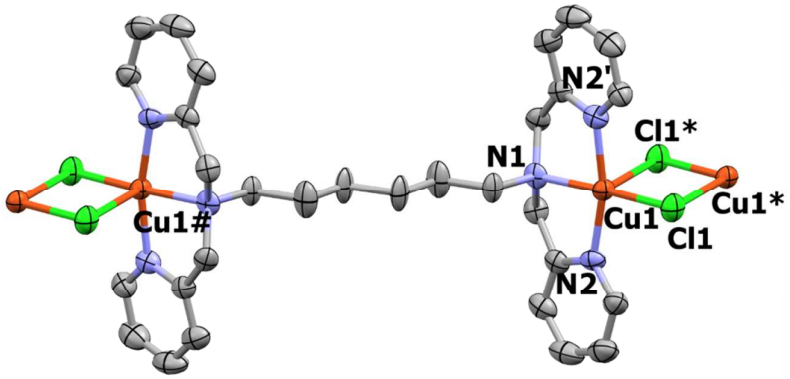

Figure 4: Displacement ellipsoid plot (50% probability level) of the cationic part of $[Cu^{II}_2(\mathbf{L^1C_6L^1})(Cl)_2]_n(BF_4)_{2n}$. Non-coordinating BF_4^- counterions, acetonitrile solvent molecules and hydrogen atoms are omitted for clarity. Symmetry operation * = [1–x, y, 1–z]; # = [–x, y, –1–z]; ‘ = [x, –y, z].

Table 3: Selected bond distances (Å) and bond angles (°) for $[Cu^{II}(\mathbf{L^1SCH_3})(Cl)](BF_4)$, $[Cu^{II}(\mathbf{L^3SCH_3})(Cl)](BF_4)$ and $[Cu^{II}(\mathbf{L^1NH_2})(Cl)](BF_4)$.

	$[Cu^{II}(\mathbf{L^1SCH_3})(Cl)](BF_4)$	$[Cu^{II}(\mathbf{L^3SCH_3})(Cl)](BF_4)$	$[Cu^{II}(\mathbf{L^1NH_2})(Cl)](BF_4)$
Cu1 - Cu1*	3.8192(3)		
Cu1 - S1/N2	2.7152(4)	2.5817(4)	2.0593(15)
Cu1 - N1	2.0558(10)	2.0876(12)	2.0439(12)
Cu1 - N11	1.9782(11)	1.9914(12)	2.1158(13)
Cu1 - N21	1.9845(11)	1.9935(13)	2.0410(13)
Cu1 - Cl1	2.2588(3)	2.2674(4)	2.2381(4)
Cu1 - Cl1*	3.1018(4)		
S1/N2 - Cu1 - N1	85.93(3)	85.75(3)	84.73(5)
S1/N2 - Cu1 - N11	101.67(3)	93.86(4)	109.75(6)
S1/N2 - Cu1 - N21	84.59(3)	82.92(4)	127.21(6)
S1/N2 - Cu1 - Cl1	100.430(11)	141.526(16)	96.44(4)
N1 - Cu1 - N11	82.43(4)	82.13(5)	80.25(5)
N1 - Cu1 - N21	83.42(4)	83.00(5)	81.87(5)
N1 - Cu1 - Cl1	173.64(3)	132.50(4)	177.49(4)
N11 - Cu1 - N21	164.06(4)	164.98(5)	117.72(5)
N11 - Cu1 - Cl1	96.15(3)	95.44(4)	97.26(4)
N21 - Cu1 - Cl1	97.09(3)	96.15(4)	99.12(4)

Symmetry operation * = [1–x, 2–y, 1–z]

The structure of $[Cu^{II}(\mathbf{L^1SCH_3})(Cl)](BF_4)$ is mostly ordered. The BF_4^- counterion is disordered over two orientations, and the occupancy factor of the major component refines to 0.70(3). The copper ion has square-pyramidal geometry ($\tau = 0.16$),[30] but the complex can also be considered a dimer when the chloride ions that bridge between two copper ions are taken into account, thus creating an octahedral environment with Cl1* and S1 on the elongated Jahn-Teller axis (Cu1-S1 2.7152(4) Å; Cu1-Cl1* 3.1018(4) Å). The Cu1-Cu1* distance of 3.8192(3) Å is larger than in the polymeric species discussed above. Formation of such dimeric structures is also observed for $[Cu^{II}(\mathbf{L^2SCH_3})(Cl)](BF_4)$, $[Cu^{II}(\mathbf{L^1*SCH_3})(Cl)](BF_4)$ and $[Cu^{II}(\mathbf{L^1*SCH_3})(Cl)]_2(CuCl_4)$ (Supporting Information). The

compounds [Cu^{II}(**L^3SCH_3**)(Cl)](BF_4) and [Cu^{II}(**L^1NH_2**)(Cl)](BF_4) do not form dimeric species, as their coordination geometry is more distorted towards trigonal bipyramidal with τ parameters of 0.39 and 0.84, respectively. In [Cu^{II}(**L^1NH_2**)(Cl)](BF_4) the Cl^- ion and the tertiary nitrogen atom occupy the axial coordination sites, whereas in [Cu^{II}(**L^3SCH_3**)(Cl)](BF_4) these positions are occupied by the pyridyl nitrogens. A structure similar to [Cu^{II}(**L^1NH_2**)(Cl)](BF_4) has been reported in the literature with ClO_4^- instead of BF_4^- as the non-coordinating counterion.[31]

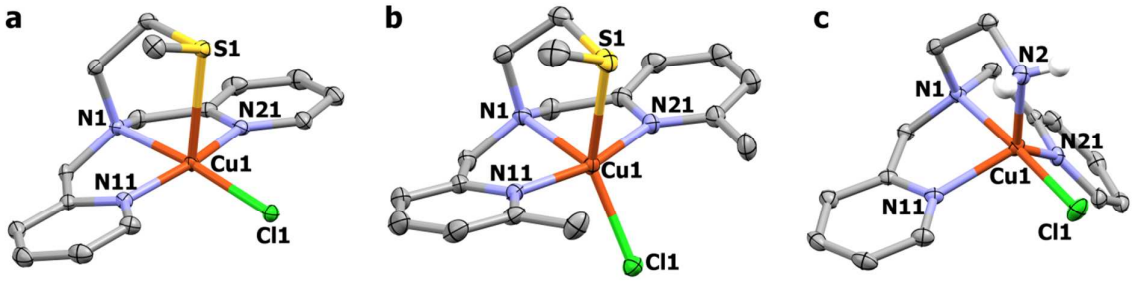

Figure 5: Displacement ellipsoid plots (50% probability level) of the cationic parts of (a) [Cu^{II}(**L^1SCH_3**)(Cl)](BF_4), (b) [Cu^{II}(**L^3SCH_3**)(Cl)](BF_4) and (c) [Cu^{II}(**L^1NH_2**)(Cl)](BF_4). The non-coordinating counterions and most of the hydrogen atoms are omitted for clarity.

2.3 Catechol Oxidation

The synthesized complexes were tested for their catalytic activity in the oxidation of 3,5-DTBC to 3,5-DTBQ. The rate of oxidation was determined by monitoring the absorbance of 3,5-DTBQ at 400 nm. All catalytic experiments were conducted at 25 °C whilst stirring and bubbling a mixture of N_2 and O_2 (1:1) through the solution; the amount of O_2 supplied in the reactions was not rate-limiting as small changes in the rate of dioxygen flow did not result in noticeable differences in the initial TOFs. A copper concentration of 0.4 mM, corresponding with 0.4 mM of a mononuclear complex or 0.2 mM of a dinuclear complex, was used together with 20 mM 3,5-DTBC. Upon addition of 20 mM NEt_3 the conversion of 3,5-DTBC started; the final solution thus contained a 1:50:50 ratio of [Cu]:substrate:base. The results of the catalytic experiments are collected in Table 4. Three different types of conversion curves were observed (A, B and C; Figure 6). Depending on the type of catalyst the oxidation rate was constant, increasing, or decreasing over time. For this reason both the maximum turnover frequencies (TOFs) and initial TOFs are reported in Table 4. After addition of NEt_3, an abrupt increase in the absorption at 400 nm was observed for all copper complexes with one Cl^- and one BF_4^- counterion (Figure 6). The height of this 'jump' was dependent on the catalyst used and appeared to be related to the presence of chloride ions (see below). The initial TOF was determined by taking the tangent of the curve of the first two seconds after the 'jump' in the absorption curve. Blank reactions were performed in the presence and absence of copper (entry 1-2, Table 4). The blank reaction with copper was performed using a 1:1 mixture in acetonitrile of [$Cu^{II}(H_2O)_6$](BF_4)$_2$ and

$CuCl_2 \cdot 2\ H_2O$ from which most of the H_2O content was removed by addition of Na_2SO_4. The catalytic activity of the copper complexes with mononucleating ligands is not much higher than for the system containing just the copper salts (entry 2 and 16-24, Table 4). In contrast, a number of the dinucleating ligands result in catalytic systems with significantly higher activity, which we will further elaborate on.

Table 4: Turnover frequencies of the oxidation of 3,5-DTBC to 3,5-DTBQ catalyzed by copper complexes with different ligands.[a]

	Ligand	Catalyst	Graph type[c]	max TOF (h^{-1})[d]	initial TOF (h^{-1})
1	-	no catalyst	C	170	15
2	-	$[Cu^{II}(Cl)](BF_4)$[b]	C	450	180
3	**L^1SSL^1**	$[Cu^{II}_2(Ligand)(Cl)_2]_n(BF_4)_{2n}$	A	-	2150
4	**L^1*SSL^1***	$[Cu^{II}_2(Ligand)(Cl)_2]_n(BF_4)_{2n}$	A	-	4700
5	**L^2SSL^2**	$[Cu^{II}_2(Ligand)(Cl)_2]_n(BF_4)_{2n}$	A	-	570
6	**L^2*SSL^2***	$[Cu^{II}_2(Ligand)(Cl)_2]_n(BF_4)_{2n}$	A	-	1750
7	**L^3SSL^3**	$[Cu^{II}_2(Ligand)(Cl)_2]_n(BF_4)_{2n}$	C	240	190
8	**L^4SSL^4**	$[Cu^{II}_2(Ligand)(Cl)_2]_n(BF_4)_{2n}$	A	-	3200
9	**L^5SSL^5**	$[Cu^{II}_2(Ligand)(Cl)_2]_n(BF_4)_{2n}$[b]	C	310	120
10	**L^1SXSL^1**	$[Cu^{II}_2(Ligand)(Cl)_2]_n(BF_4)_{2n}$	C	430	330
11	**L^1SL^1**	$[Cu^{II}_2(Ligand)(Cl)_2]_n(BF_4)_{2n}$	A	-	1800
12	**$L^1C_6L^1$**	$[Cu^{II}_2(Ligand)(Cl)_2]_n(BF_4)_{2n}$	A	-	530
13	**L^1PhL^1**	$[Cu^{II}_2(Ligand)(Cl)_2]_n(BF_4)_{2n}$	C	580	190
14	**$L^{Pz}SSL^{Pz}$**	$[Cu^{II}_2(Ligand)(Cl)_2]_n(BF_4)_{2n}$	C	390	240
15	**$L^{MPz}SSL^{MPz}$**	$[Cu^{II}_2(Ligand)(Cl)_2]_n(BF_4)_{2n}$	C	390	170
16	**Py_3N**	$[Cu^{II}(Ligand)(Cl)](BF_4)$	A	-	600
17	**L^1SCH_3**	$[Cu^{II}(Ligand)(Cl)](BF_4)$	A	-	760
18	**L^1*SCH_3**	$[Cu^{II}(Ligand)(Cl)](BF_4)$	C	480	370
19	**L^2SCH_3**	$[Cu^{II}(Ligand)(Cl)](BF_4)$	C	330	150
20	**L^3SCH_3**	$[Cu^{II}(Ligand)(Cl)](BF_4)$	C	220	110
21	**L^1OH**	$[Cu^{II}(Ligand)(Cl)](BF_4)$	B	-	430
22	**L^1NH_2**	$[Cu^{II}(Ligand)(Cl)](BF_4)$	B	-	340
23	**Py_2NH**	$[Cu^{II}(Ligand)(Cl)](BF_4)$	A	-	440
24	**Py_2S**	$[Cu^{II}(Ligand)(Cl)](BF_4)$	C	390	160

[a] Reaction conditions: [Cu] = 0.4 mM; 3,5-DTBC/NEt_3/Cu = 50/50/1; 3 mL CH_3CN. TOFs were determined from the change in absorbance of 3,5-DTBQ at 400 nm.

[b] Complex was formed in situ.

[c] The three different types of graphs A, B and C are depicted in Figure 6.

[d] Only given when maximum TOF is higher than initial TOF (graph type C).

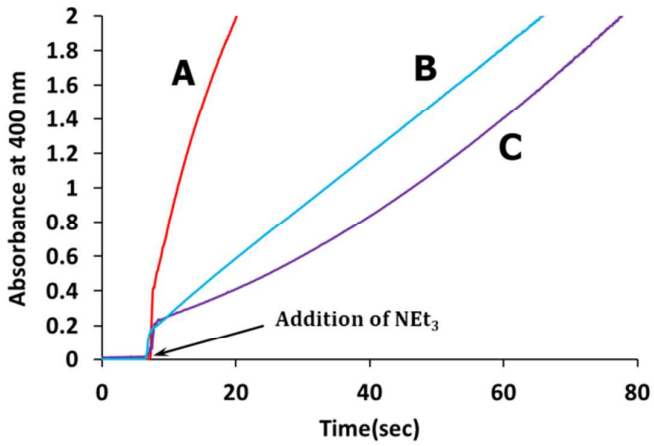

Figure 6: Development in time of the absorption at 400 nm due to 3,5-DTBQ formation, catalyzed by $[Cu^{II}_2(\mathbf{L^1SSL^1})(Cl)_2](BF_4)_2$ (red, type A), $[Cu^{II}(\mathbf{L^1OH})(Cl)](BF_4)$ (blue, type B) and $[Cu^{II}_2(\mathbf{L^{Pz}SSL^{Pz}})(Cl)_2](BF_4)_2$ (purple, type C).

The catalytic system comprising the ligand $\mathbf{L^1SSL^1}$ shows reasonably high activity (entry 3), but introduction of methyl groups at the *ortho*-position of the pyridyl rings results in a considerable decrease of the catalytic activity (entry 3, 5 and 7). Addition of a methyl group next to the sulfur in the disulfide bond, however, results in significantly higher activity (entry 3-4, 5-6). Changing the bridge between the tertiary amine and the pyridyl groups from a methylene to an ethylene spacer at two positions leads to an increase in activity (entry 3 vs 8), but at four positions it leads to a dramatic decrease in activity (entry 3 vs 9). The use of pyridyl-containing ligands containing a disulfide bond generally results in higher TOFs, but the high catalytic activity of the system comprising $\mathbf{L^1SL^1}$ indicates that the presence of a thioether instead of a disulfide group can give similar performance (entry 3 vs 11). The presence of an S-donor atom in the ligand does have a positive effect on the catalytic activity of the system, considering that a similar complex with an alkane bridge ($\mathbf{L^1C_6L^1}$) shows a significantly lower TOF (entry 3 vs 12). The complex with ligand $\mathbf{L^1SXSL^1}$ has considerably lower activity than the compound with $\mathbf{L^1*SSL^1*}$, while these systems only differ in the rigidity of the ligand (entry 4 vs 10). Such rigidity might also be a factor in the low activity of the complex with $\mathbf{L^1PhL^1}$ (entry 13). The presence of pyrazole moieties instead of pyridyl groups stabilizes the Cu^I oxidation state,[24] which is reflected in the negative effect on the catalytic activity (entry 14-15).

The catalytic activity decreases with increasing concentration of chloride ions, as can be seen in Table 5. The absorption spectra for $[Cu^{II}_2(\mathbf{L^{Pz}SSL^{Pz}})]^{4+}$ with 1-5 equivalents of chloride ions (in ratio to the dinuclear complex) have been recorded. The spectroscopic changes that are observed upon addition of 1-4 equivalents of chloride ions indicate coordination of the chloride ions to the copper center. During catalysis, the coordinated chloride ions will hamper binding of the substrate or activation of dioxygen. Addition of a fifth equivalent of Cl^- results in formation of an absorption band at 460 nm, which can be attributed to the formation of the complex anion $CuCl_4^{2-}$ (Figure S9).[32-34] As mentioned before, an

abrupt increase is observed in the absorption at 400 nm at the start of the reaction. This 'jump' is likely caused by a change in absorption spectrum when the chloride ions dissociate from the copper center. In other words, the change in absorption at 400 nm can be attributed to a change in the $Cu^{II} \leftarrow Cl$ LMCT. This conclusion is in agreement with the absence of the 'jump' when the 3,5-DTBC oxidation is carried out in either the presence of an excess of chloride ions or the absence of chloride ions (Figure S10). It is clear that when chloride ions are not present in solution, the change in LMCT will not occur. In the presence of an excess of chloride ions, part of the copper centers dissociate from the ligand to form $CuCl_4^{2-}$ complex anions. Chloride dissociation is suppressed by the excess of chloride ions, resulting in the absence of an abrupt 'jump' in the absorption curve and leading to lower activity.

Table 5: Turnover frequencies of the oxidation of 3,5-DTBC to 3,5-DTBQ catalyzed by $[Cu^{II}_2(\mathbf{L^{Pz}SSL^{Pz}})]^{4+}$ in the presence of different chloride concentrations.[a]

Catalyst	Graph type[c]	max. TOF (h^{-1})	initial TOF (h^{-1})	Cl^- conc (mM)
$[Cu^{II}_2(\mathbf{L^{Pz}SSL^{Pz}})](BF_4)_4$[b]	C	550	220	0
$[Cu^{II}_2(\mathbf{L^{Pz}SSL^{Pz}})(Cl)_2](BF_4)_2$	C	390	240	0.4
$Cu^{II}_2(\mathbf{L^{Pz}SSL^{Pz}})Cl_4$[b]	C	360	140	0.8
$[Cu^{II}_2(\mathbf{L^{Pz}SSL^{Pz}})(Cl)_2](BF_4)_2 + Bu_4NCl$	C	230	100	20

[a] Reaction conditions: [Cu] = 0.4 mM; 3,5-DTBC/NEt_3/Cu = 50/50/1; 3 mL CH_3CN. TOFs were determined from the change in absorbance of 3,5-DTBQ at 400 nm.
[b] Complex was formed in situ
[c] The three different types of graphs A, B and C are depicted in Figure 6.

The catalytic system obtained with $[Cu^{II}_2(\mathbf{L^1{*}SSL^1{*}})(Cl)_2]_n(BF_4)_{2n}$ shows the highest initial TOF with 4700 turnovers h^{-1} (entry 4). To acquire insight into the kinetics of the 3,5-DTBC oxidation by $[Cu^{II}_2(\mathbf{L^1{*}SSL^1{*}})(Cl)_2]_n(BF_4)_{2n}$ the substrate concentration was varied; the results of these experiments are shown in Figure 7. The plot shows a first-order rate dependence on the substrate at lower 3,5-DTBC concentrations, but at higher concentrations the Cu^{II} complex exhibits saturation. We have applied the Michaelis-Menten model to plot a Lineweaver-Burk graph (inset Figure 7) from which the maximum rate (V_{max} = 0.29 mM s^{-1}) and the Michaelis-Menten constant (K_m = 2.2 mM) can be obtained. From these data the k_{cat} is calculated to be 5200 h^{-1}, which indicates that a small increase in initial TOF can be gained when the substrate concentration is increased (3,5-DTBC/Cu > 50). A comparable plot was obtained for the mononuclear complex $[Cu^{II}(\mathbf{L^1SCH_3})(Cl)](BF_4)$, which showed similar behavior as $[Cu^{II}_2(\mathbf{L^1{*}SSL^1{*}})(Cl)_2]_n(BF_4)_{2n}$, but with a lower V_{max} (0.05 mM s^{-1}) and higher K_m value (5.3 mM) (Figure S12). As it was found that the presence of chloride ions has a negative effect on the catalytic activity of the catalyst (Table 5), the concentration dependence of the catalytic system comprising $\mathbf{L^1{*}SSL^1{*}}$ in the absence of chlorides was also investigated. The compound $[Cu^{II}_2(\mathbf{L^1{*}SSL^1{*}})](BF_4)_4$ was formed in situ by adding two equivalents of $[Cu^{II}(H_2O)_6](BF_4)_2$ to $\mathbf{L^1{*}SSL^1{*}}$ and removing most of the H_2O with Na_2SO_4. The Lineweaver-Burk plot (Figure S13) for

this catalyst shows a high V_{max} of 0.38 mM s^{-1} from which a k_{cat} of 6900 h^{-1} can be calculated. At lower catalyst concentrations the catalyst seems to be rapidly deactivated (Figure S11).

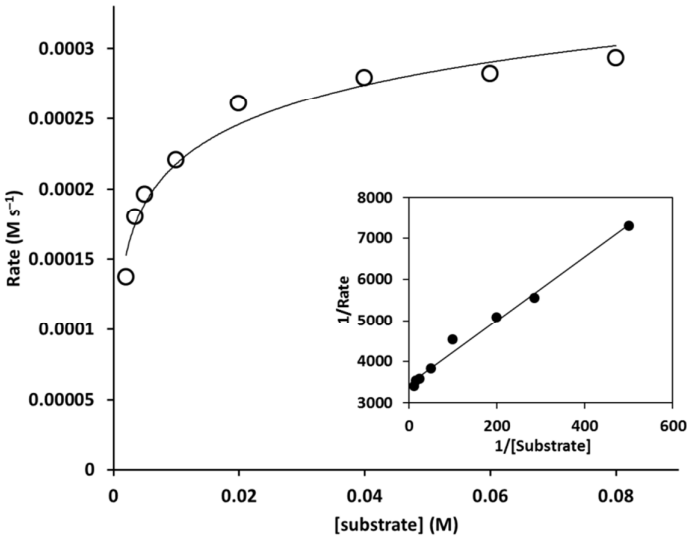

Figure 7: A plot of the substrate concentration vs the catalytic rate for $[Cu^{II}_2(\mathbf{L^1*SSL^1*})(Cl)_2](BF_4)_2$. The inset shows the Lineweaver-Burk plot. Reaction conditions: 0.4 mM [Cu], 20 mM NEt_3 and varying amounts of 3,5-DTBC in 3 mL CH_3CN. V_{max} = 0.29 mM s^{-1}; K_m = 2.2 mM; k_{cat} = 5200 h^{-1}.

3. Discussion

A large library of Cu^{II} complexes has been synthesized and investigated for their catalytic activity in the oxidation of 3,5-DTBC. Crystal structures of a number of the Cu^{II} complexes of dinucleating ligands show that in these cases the chloride ions bridge between the Cu^{II} centers of neighboring molecules, forming polymeric chains. The Cu^{II} complexes with mononucleating ligands form dimeric species in some cases, depending on the coordination geometry of the copper ion. A square-pyramidal geometry of the copper center leaves the sixth coordination site open for coordination to the chloride ion of a molecule in a neighboring subunit.

The oxidation of 3,5-DTBC was carried out with different catalytic systems; three types of reactivity were observed with an increasing, decreasing or constant oxidation rate (Figure 6). This variance in catalyst behavior indicates that depending on the ligand different activation mechanisms are operative in the formation of the active species. Catalytic systems that show development of the product following type A have the highest activity at the start of the experiment and become slower over time. For the less active catalytic systems, this type of behavior indicates catalyst degradation over time. However, for the faster catalytic systems like $[Cu^{II}_2(\mathbf{L^1*SSL^1*})](BF_4)_4$, the decrease in the catalytic rate may also be due to depletion of the substrate. The catalysts containing $\mathbf{L^1OH}$ and $\mathbf{L^1NH_2}$ show constant activity during the entire experiment (type B), indicating that there is no deactivation of the

catalyst. All the other catalysts show an induction period in their activity (type C), which indicates the presence of a pre-catalyst at the beginning of the reaction that is converted to the active catalyst (possibly a Cu^{II} μ-hydroxo species) later on. The ligands **L^1OH** and **L^1NH_2** contain a proton donor/acceptor moiety, which might explain the absence of a similar induction period for these catalysts.

The presence of chloride ions has a negative effect on the catalytic activity. The chloride ions inhibit the reaction either by competing with the substrate for coordination sites or by formation of $CuCl_4^{2-}$, resulting in lower concentration of the active species in solution. The ease of formation of $CuCl_4^{2-}$ is demonstrated by the structure of the compound $[Cu^{II}(\mathbf{L^1{*}SCH_3})(Cl)]_2(CuCl_4)$, which even formed in the presence of a substoichiometric amount of copper (Figure S4). Similar behavior was observed for **L^1SXSL^1**.[24]

When comparing the catalytic rates of the different systems (Table 4), it is clear that many of the systems under study are not (much) more active than the blank system comprising copper salts in the absence of a ligand. The relative differences however, are very large. The mononuclear catalysts generally have a lower initial TOF than the catalysts with dinucleating ligands, which is not surprising considering that the reaction requires two electrons and that the active species has been proposed to be dinuclear.[15] A number of the systems containing dinucleating ligands behave as mononuclear catalysts, because they are either too rigid (**L^1SXSL^1** entry 10, and **L^1PhL^1** entry 13) or lack bridging sulfur donor atoms (**$L^1C_6L^1$** entry 12) and therefore exhibit lower TOFs. Several other of the dinucleating ligands strongly stabilize the Cu^I oxidation state, and thus also result in low activity (entry 7, 9, 14 and 15).[7, 8] The catalytic systems with the highest activity are those containing ligands that stabilize Cu^{II} μ-thiolate complexes (**L^1SSL^1**, **$L^1{*}SSL^1{*}$**, **L^2SSL^2**, **$L^2{*}SSL^2{*}$**, **L^4SSL^4**).[4, 7, 8, 35] The compound $[Cu^{II}_2(\mathbf{L^2SSL^2})(Cl)_2]_n(BF_4)_{2n}$ forms an exception with its relatively low activity, which can be explained by the fact that **L^2SSL^2** in CH_3CN, the solvent used for catalysis, stabilizes a Cu^I disulfide complex rather than a Cu^{II} μ-thiolate complex.[8] The k_{cat} of 6900 h^{-1} observed for $[Cu^{II}_2(\mathbf{L^1{*}SSL^1{*}})](BF_4)_4$ is the second highest rate reported for 3,5-DTBC oxidation in CH_3CN thus far.[16, 36]

The existence of an equilibrium between dinuclear Cu^I-disulfide compounds and the redox isomeric dinuclear Cu^{II} μ-thiolate compounds has been shown to be strongly dependent on the redox potential of these compounds, as induced by the electronic and steric properties of the ligand system.[24] Similarly, it may be argued that the high activity of the systems with Cu^{II} μ-thiolate stabilizing ligands stems from the redox potential of the Cu^I intermediate and the ability of these complexes to stabilize a $Cu^{II}_2(\mu\text{-}\eta^2\text{:}\eta^2\text{-peroxide})$ species that is structurally as well as electronically similar to the Cu^{II} μ-thiolate complex (Figure 1). Stabilization of the $Cu^{II}_2(\mu\text{-}\eta^2\text{:}\eta^2\text{-peroxide})$ species may be the prime reason for a faster reaction of the dinuclear Cu^I intermediate with O_2, thus resulting in efficient Cu^I to Cu^{II} reoxidation. As the reoxidation of the Cu^I species has been proposed to be the rate-determining step of the reaction, this will thus result in an increase of the overall reaction rate.[14, 17, 37] The activity of these

catalytic systems can probably be increased even further by using a protic solvent like methanol, but this might also result in faster catalyst degradation. If via the redox equilibrium the Cu^{I} disulfide intermediate is transformed to the corresponding Cu^{II} thiolate species this will most likely lead to rapid catalyst deactivation, since Cu^{II} μ-thiolate complexes have been reported either to be oxidized to Cu^{II} sulfinate and sulfonate complexes or to react with the substrate.[19, 38]

4. Conclusion

Cu^{II} complexes have been synthesized comprising either mononucleating or dinucleating ligands for the catalytic oxidation of 3,5-DTBC. Very high activity for the oxidation of 3,5-DTBC is achieved using ligands that have the ability to form Cu^{II} μ-thiolate complexes. The presence of chloride ions has a negative effect on the catalytic rates because of coordination to the active sites or the formation of $Cu^{II}Cl_4^{2-}$. The highest TOF reached is 6900 h^{-1} using $[Cu^{II}_2(\mathbf{L^1{*}SSL^1{*}})](BF_4)_4$, which is one of the highest TOFs reported for 3,5-DTBC oxidation in CH_3CN thus far. These results show that there are similarities between thiolato copper and (per)oxido copper chemistry and that ligands that stabilize Cu^{II} μ-thiolate complexes might also induce the rapid formation of $Cu^{II}_2(\mu\text{-}\eta^2\text{:}\eta^2\text{-peroxide})$ species.

5. Experimental Section

5.1 General Methods

Reagents and solvents were purchased from commercial sources. $\mathbf{L^1SSL^1}$, $\mathbf{L^3SSL^3}$, $\mathbf{L^5SSL^5}$,[7] $\mathbf{L^2SSL^2}$, $\mathbf{L^4SSL^4}$,[8] $\mathbf{L^1{*}SSL^1{*}}$, $\mathbf{L^2{*}SSL^2{*}}$,[4] $\mathbf{L^1SXSL^1}$, $\mathbf{L^{Pz}SSL^{Pz}}$, $\mathbf{L^{MPz}SSL^{MPz}}$, $[Cu^{II}_2(\mathbf{L^{Pz}SSL^{Pz}})(Cl)_2]_n(BF_4)_{2n}$, $[Cu^{II}_2(\mathbf{L^{MPz}SSL^{MPz}})(Cl)_2]_n(BF_4)_{2n}$,[24] $\mathbf{L^1C_6L^1}$,[20] $\mathbf{L^1PhL^1}$,[21, 22] $\mathbf{Py_3N}$,[23] $\mathbf{L^1NH_2}$[31] and 1,5-diamino-3-thiapentane dihydrobromide[28] were synthesized according to literature procedures. NMR spectra were recorded on a Bruker 300 DPX spectrometer. IR spectra were obtained on a Perkin Elmer UATR (Single Reflection Diamond) Spectrum Two device (4000-700 cm^{-1}; resolution 4 cm^{-1}). Mass spectrometry was measured using a Finnigan Aqua Mass Spectrometer (MS) with electro spray ionization (ESI). Sample introduction was achieved through a Dionex ASI-100 automated sample injector with an eluent flow rate of 0.2 mL/min. Elemental analyses were performed using a Perkin Elmer 2400 Series II CHNS/O analyzer or were performed by the Microanalytical laboratory Kolbe in Germany. UV-vis absorbance spectra were recorded on a Varian Cary50 spectrophotometer or using a transmission dip probe with variable path length on an Avantes Avaspec-2048 spectrometer with Avalight-DH-S-BAL light source.

5.2 X-ray Crystallography

$[Cu^{II}_2(\mathbf{L^1SL^1})(Cl)_2]_n(BF_4)_{2n}$ and $[Cu^{II}(\mathbf{L^1NH_2})(Cl)](BF_4)$

The reflection intensities for $[Cu^{II}_2(\mathbf{L^1SL^1})(Cl)_2]_n(BF_4)_{2n}$ and $[Cu^{II}(\mathbf{L^1NH_2})(Cl)](BF_4)$ were measured at 110(2) K using a KM4/Xcalibur (detector: Sapphire3) with enhanced graphite-monochromated Mo *K*α radiation (λ = 0.71073 Å) under the program CrysAlisPro (Version 1.171.36.24 Agilent Technologies, 2012). The same program was used to refine the cell dimensions and for data reduction. The structures were solved with the

program SHELXS-97/SHELXS-2013 (Sheldrick, 2008/2013)[39] and was refined on F^2 with SHELXL-97/SHELXL-2013 (Sheldrick, 2008/2013).[39] Analytical numeric absorption corrections based on a multifaceted crystal model were applied using CrysAlisPro. The temperature of the data collection was controlled using the system Cryojet (manufactured by Oxford Instruments). The H atoms were placed at calculated positions using the instructions AFIX 23, AFIX 43 or AFIX 137 with isotropic displacement parameters having values 1.2 or 1.5 times *U*eq of the attached C atoms. The H atoms attached to N2 of $[Cu^{II}(\mathbf{L^1NH_2})(Cl)](BF_4)$ were found from difference Fourier map, and their coordinates and isotropic temperature factors were refined freely. CCDC 1043171 and 1043165 contain the supplementary crystallographic data for $[Cu^{II}_2(\mathbf{L^1SL^1})(Cl)_2]_n(BF_4)_{2n}$ and $[Cu^{II}(\mathbf{L^1NH_2})(Cl)](BF_4)$. This data can be obtained free of charge from The Cambridge Crystallographic Data Centre via www.ccdc.cam.ac.uk/data_request/cif.

$[Cu^{II}(\mathbf{L^1SCH_3})(Cl)](BF_4)$ and $[Cu^{II}(\mathbf{L^3SCH_3})(Cl)](BF_4)$

The reflection intensities for $[Cu^{II}(\mathbf{L^1SCH_3})(Cl)](BF_4)$ and $[Cu^{II}(\mathbf{L^3SCH_3})(Cl)](BF_4)$ were measured at 110(2) K using a SuperNova diffractometer (equipped with Atlas detector) with Mo *K*α radiation (λ = 0.71073 Å) for $[Cu^{II}(\mathbf{L^1SCH_3})(Cl)](BF_4)$ and Cu *K*α radiation (λ = 1.54178 Å) for $[Cu^{II}(\mathbf{L^3SCH_3})(Cl)](BF_4)$ under the program CrysAlisPro (Version 1.171.36.32 Agilent Technologies, 2013). The same program was used to refine the cell dimensions and for data reduction. The structures were solved with the program SHELXS-2013 (Sheldrick, 2013)[39] and were refined on F^2 with SHELXL-2013 (Sheldrick, 2013).[39] Analytical numeric absorption corrections based on a multifaceted crystal model were applied using CrysAlisPro. The temperature of the data collection was controlled using the system Cryojet (manufactured by Oxford Instruments). The H atoms were placed at calculated positions using the instructions AFIX 23, AFIX 43 or AFIX 137 with isotropic displacement parameters having values 1.2 or 1.5 times *U*eq of the attached C atoms. CCDC 1043166 and 1043170 contain the supplementary crystallographic data for $[Cu^{II}(\mathbf{L^1SCH_3})(Cl)](BF_4)$ and $[Cu^{II}(\mathbf{L^3SCH_3})(Cl)](BF_4)$.

$[Cu^{II}_2(\mathbf{L^1C_6L^1})(Cl)_2]_n(BF_4)_{2n}$

The reflection intensities for $[Cu^{II}_2(\mathbf{L^1C_6L^1})(Cl)_2]_n(BF_4)_{2n}$ were measured on a Bruker Kappa Apex II diffractometer with sealed tube and Triumph monochromator (λ = 0.71073 Å) up to a resolution of $(\sin\theta/\lambda)_{max}$ = 0.57 $Å^{-1}$. The crystal consisted of several fragments. The four major fragments were taken into account during the integration with the Eval14 software.[40] The second fragment has an arbitrary orientation with respect to the first. The third fragment is generated by a twofold rotation about hkl=(1,0,0) from the first. The fourth fragment has the same twin relation to the second. An absorption correction based on multiple measured reflections was performed with TWINABS (0.57-0.75 correction range).[41] The structure was solved with Direct Methods using SHELXS-97 and refined with SHELXL-97 against F^2 of all reflections.[39] The presence of four fragments was handled with a HKLF-5 reflection file.[42] The twin fractions refined to 0.342(15), 0.267(7), and 0.083(4). Non-hydrogen atoms were refined freely with anisotropic displacement parameters. Hydrogen atoms were introduced in calculated positions and refined with a riding model. The BF_4^- anion was refined with a disorder model of two orientations. Geometry calculations and checking for higher symmetry was performed with the PLATON program.[43] CCDC 1042477 contains the supplementary crystallographic data for $[Cu^{II}_2(\mathbf{L^1C_6L^1})(Cl)_2]_n(BF_4)_{2n}$.

5.3 Ligand Synthesis

*Bis-1,5-((2-pyridylmethyl)amino)ethyl-3-thiapentane (**L^1SL^1**)*

1,5-Diamino-3-thiapentane dihydrobromide (1.43 g, 5.1 mmol) was dissolved in methanol (40 mL). To this solution 2-pyridinecarboxaldehyde (1.9 mL, 20.3 mmol) was added, after which the reaction mixture was cooled to 0 °C. $NaBH_3CN$ (1.28 g, 20.3 mmol) was added in small portions. The reaction mixture was allowed to warm up to RT and was stirred for 3 days. The reaction mixture was quenched by addition of HCl (37%) until pH = 1. After evaporation of the solvent, the product was treated with NaOH (50 mL; 5 M) and the aqueous layer was extracted with $CHCl_3$ (3 x 25 mL). The organic fractions were combined, dried over $MgSO_4$ and evaporated to dryness yielding **L^1SL^1** as a brown oil (1.68 g, 3.5 mmol, 68%). ^{1}H NMR (300 MHz, CD_3OD, RT): δ 2.64 (m, 8H, S-CH_2-CH_2), 3.76 (s, 8H, Py-CH_2-N), 7.21 (m, 4H, Py-H_5), 7.62 (d, J = 8 Hz, 4H, Py-H_3), 7.72 (dt, J = 8 Hz, 2 Hz, 4H, Py-H_4), 8.41 (m, 4H, Py-H_6). ^{13}C NMR (75 MHz, CD_3OD, RT): δ 30.5 (S-CH$_2$-CH$_2$), 55.1 (S-CH$_2$-CH$_2$), 60.7 (Py-CH$_2$-N), 123.6 (Py-C_5), 124.6 (Py-C_3), 138.4 (Py-C_4), 149.3 (Py-C_6), 160.4 (Py-C_2). ESI-MS found (calculated) for $[M + H]^+$ *m/z* 485.1 (485.3); $[M + Na]^+$ *m/z* 507.1 (507.2). IR (neat, cm^{-1}): 3050*w*, 2924*w*, 2821*m*, 1589*s*, 1569*m*, 1473*m*, 1432*s*, 1362*m*, 1265*w*, 1147*m*, 1117*m*, 1086*m*, 1047*m*, 994*m*, 978*m*, 895*w*, 755*vs*, 731*vs*, 701*m*, 613*m*, 465*w*.

L^1*SCH$_3$

A mixture of bis(2-pyridylmethyl)amine (1.44 mL, 8.0 mmol) and propylene sulfide (0.94 mL, 12.0 mmol) was stirred in 20 mL CH_3CN at reflux temperature for 18 hrs under Ar atmosphere. The solvent was evaporated, after which the resulting oil was dissolved in 20 mL tetrahydrofuran. NaH (0.37 g, 9.3 mmol, 60% in mineral oil) was added and the reaction mixture was stirred for 2 hrs. To this pink reaction mixture, MeI (0.51 mL, 8.2 mmol) was added and all was stirred for 5 hrs. The reaction was quenched by dropwise addition of H_2O. In total 40 mL H_2O was added after which the water layer was extracted with CH_2Cl_2 (3 × 30 mL). The combined organic layers were dried over Na_2SO_4. The crude product was purified by column chromatography over basic alumina (50/50 EtOAc/petroleum ether) to yield **L^1*SCH$_3$** as a light yellow oil (1.98 g, 6.9 mmol, 86%). ^{1}H NMR (300 MHz, CD_3OD, RT): δ 1.18 (s, 1.5H, C*-CH_3), 1.20 (s, 1.5H, C*-CH_3), 1.99 (s, 3H, S-CH_3), 2.52 (dd, J = 13 Hz, 8 Hz, 1H, N-CH_2-C*), 2.68 (dd, J = 13 Hz, 7 Hz, 1H, N-CH_2-C*), 2.86 (dt, J = 8 Hz, 7 Hz, 1H, C*-H), 3.81 (s, 4H, Py-CH_2-N), 7.30 (ddd, J = 7 Hz, 5 Hz, 1 Hz, 2H, Py-H_5), 7.71 (d, J = 8 Hz, 2H, Py-H_3), 7.82 (td, J = 8 Hz, 2 Hz, 2H, Py-H_4), 8.43 (ddd, J = 5 Hz, 2 Hz, 1 Hz, 2H, Py-H_6). ^{13}C NMR (75 MHz, CD_3OD, RT): δ 13.0 (S-CH$_3$), 19.5 (C*-CH$_3$), 40.3 (*C**), 61.4 (N-CH$_2$-C*), 61.5 (Py-CH$_2$-N), 123.8 (Py-C_5), 125.1 (Py-C_3), 138.5 (Py-C_4), 149.3 (Py-C_6), 160.5 (Py-C_2). ESI-MS found (calculated) for $[M + H]^+$ *m/z* 288.1 (288.2). IR (neat, cm^{-1}): 3392*br*, 2961*w*, 2919*m*, 2822*w*, 1663*w*, 1589*s*, 1569*m*, 1473*m*, 1432*s*, 1365*m*, 1300*w*, 1247*w*, 1148*m*, 1125*w*, 1075*m*, 1047*m*, 995*m*, 981*m*, 957*m*, 759*vs*, 613*m*, 525*m*, 460*m*.

N-((6-methylpyridin-2-yl)methyl)-2-(methylthio)ethylamine

2-(Methylthio)ethylamine (1.00 g, 11.0 mmol) and 6-methylpyridine-2-carboxaldehyde (1.34 g, 11.0 mmol) were dissolved in 35 mL methanol and stirred at reflux temperature for 24 hrs. The dark orange solution was cooled to RT, after which $NaBH_4$ (0.64 g, 16.9 mmol) was added and the reaction mixture was stirred for 3 hrs. The solvent was evaporated and 30 mL H_2O and 30 mL CH_2Cl_2 were added. The layers were separated and the

aqueous layer was extracted CH_2Cl_2 (2 × 30 mL). The combined organic layers were dried over Na_2SO_4 and the solvent was evaporated to yield *N*-((6-methylpyridin-2-yl)methyl)-2-(methylthio)ethylamine in quantitative yield as a red/brown oil. ^{1}H NMR (300 MHz, CD_3OD, RT): δ 2.04 (s, 3H, S-CH_3), 2.52 (s, 3H, Py-CH_3), 2.65 (m, 2H, S-CH_2-CH_2), 2.79 (m, 2H, S-CH_2-CH_2), 3.85 (s, 2H, Py-CH_2-N), 7.14 (d, J = 8 Hz, 1H, Py-H_3), 7.23 (d, J = 8 Hz, 1H, Py-H_5), 7.66 (t, J = 8 Hz, 1H, Py-H_4). ^{13}C NMR (75 MHz, CD_3OD, RT): δ 15.1 (S-CH$_3$), 24.1 (Py-CH$_3$), 34.5 (S-CH$_2$-CH$_2$), 48.1 (S-CH$_2$-CH$_2$), 54.8 (Py-CH$_2$-N), 120.9 (Py-C_5), 123.1 (Py-C_3), 138.7 (Py-C_4), 159.0 (Py-C_6), 159.5 (Py-C_2).

L^{2}SCH$_3$

N-((6-methylpyridin-2-yl)methyl)-2-(methylthio)ethylamine (1.28 g, 6.5 mmol) and 2-pyridinecarboxaldehyde (0.62 mL, 6.5 mmol) were dissolved in 20 mL methanol and stirred at reflux temperature for 2 hrs. The dark brown solution was cooled to RT, $NaBH_4$ (0.39 g, 10.4 mmol) was added and the reaction mixture was stirred for 3 hrs. The solvent was evaporated and 20 mL H_2O and 20 mL CH_2Cl_2 was added. The layers were separated and the aqueous layer was extracted with CH_2Cl_2 (2 × 20 mL). The combined organic layers were dried over Na_2SO_4 and the solvent was evaporated to yield a brown oil (1.84 g). The compound was purified by column chromatography over basic alumina (30/70 EtOAc/petroleum ether) to yield **L^{2}SCH$_3$** as a yellow/orange oil (0.93 g, 3.2 mmol, 50%). ^{1}H NMR (300 MHz, CD_3OD, RT): δ 1.59 (s, 3H, S-CH_3), 2.47 (s, 3H, Py$_{Me}$-CH_3), 2.64 (m, 2H, S-CH_2-CH_2), 2.75 (m, 2H, S-CH_2-CH_2), 3.79 (s, 2H, Py-CH_2-N), 3.82 (s, 2H, Py-CH_2-N), 7.09 (d, J = 8 Hz, 1H, Py$_{Me}$-H_3), 7.24 (ddd, J = 7 Hz, 5 Hz, 1 Hz, 1H, Py$_{Me}$-H_5), 7.47 (d, J = 8 Hz, 1H, Py-H_3), 7.65 (m, 2H, Py-H_4; Py$_{Me}$-H_4), 7.77 (td, J = 8 Hz, 2 Hz, 1H, Py-H_5), 8.42 (d, J = 5 Hz, 1H, Py-H_6). ^{13}C NMR (75 MHz, CD_3OD, RT): δ 15.6 (S-CH$_3$), 23.9 (Py-CH$_3$), 32.5 (S-CH$_2$-CH$_2$), 54.7 (S-CH$_2$-CH$_2$), 60.8 (Py-CH$_2$-N), 60.8 (Py-CH$_2$-N), 121.6 (Py$_{Me}$-C_5), 123.1 (Py$_{Me}$-C_3), 123.7 (Py-C_5), 124.8 (Py-C_3), 138.5 (Py$_{Me}$-C_4), 138.7 (Py-C_4), 149.3 (Py-C_6), 158.5 (Py$_{Me}$-C_2), 159.9 (Py$_{Me}$-C_6), 160.6 (Py-C_2). ESI-MS found (calculated) for $[M + H]^+$ *m/z* 288.1 (288.2). IR (neat, cm^{-1}): 3393*w*, 3061*w*, 2916*m*, 2828*m*, 1591*s*, 1577*s*, 1456*s*, 1433*s*, 1363*m*, 1290*w*, 1152*m*, 1118*m*, 1089*m*, 1047*m*, 994*m*, 783*s*, 756*vs*, 614*m*, 545*m*.

L^{3}SCH$_3$

N-((6-methylpyridin-2-yl)methyl)-2-(methylthio)ethylamine (1.28 g, 6.5 mmol) and 6-methylpyridine-2-carboxaldehyde (0.79 g, 6.5 mmol) were dissolved in 20 mL methanol and stirred at reflux temperature for 18 hrs. The brown solution was cooled to RT and $NaBH_4$ (0.37 g, 9.8 mmol) was added and the reaction mixture was stirred for 2 hrs. The solvent was evaporated and 20 mL H_2O and 20 mL CH_2Cl_2 were added. The layers were separated and the aqueous layer was extracted two more times with 20 mL CH_2Cl_2. The combined organic layers were dried over Na_2SO_4 and the solvent was evaporated to yield a brown oil (1.93 g). The compound was purified by column chromatography over basic alumina (30/70 EtOAc/petroleum ether) to yield **L^{3}SCH$_3$** as a yellow/orange oil (0.91 g, 3.0 mmol, 46%). ^{1}H NMR (300 MHz, CD_3OD, RT): δ 1.95 (s, 3H, S-CH_3), 2.47 (s, 6H, Py-CH_3), 2.64 (m, 2H, S-CH_2-CH_2), 2.74 (m, 2H, S-CH_2-CH_2), 3.78 (s, 4H, Py-CH_2-N), 7.08 (d, J = 8 Hz, 2H, Py-H_3), 7.47 (d, J = 8 Hz, 2H, Py-H_5), 7.63 (t, J = 8 Hz, 2H, Py-H_4). ^{13}C NMR (75 MHz, CD_3OD, RT): δ 15.6 (S-CH$_3$), 23.9 (Py-CH$_3$), 32.6 (S-CH$_2$-CH$_2$), 54.7 (S-CH$_2$-CH$_2$), 60.8 (Py-CH$_2$-N), 121.5 (Py-C_5), 123.1 (Py-C_3), 138.7 (Py-C_4), 158.5 (Py-C_6), 160.1 (Py-C_2). ESI-MS found (calculated) for $[M + H]^+$ *m/z* 302.1 (302.2). IR

(neat, cm^{-1}): 3388*w*, 3061*w*, 2917*m*, 2829*w*, 1592*s*, 1577*s*, 1456*s*, 1375*m*, 1355*m*, 1291*w*, 1154*m*, 1117*m*, 1090*m*, 1035*m*, 994*m*, 972*m*, 786*s*, 760*m*, 627*m*, 546*m*.

L^1OH

This ligand was synthesized using a modified literature procedure.[23, 26] 2-Pyridinecarboxaldehyde (1.90 mL, 20.0 mmol) was added to ethanolamine (0.60 mL, 10.0 mmol) dissolved in 30 mL CH_2Cl_2. $NaBH(OAc)_3$ (6.0 g, 28.3 mmol) was added in portions over 15 min. after which the reaction mixture was stirred for 4 hrs. The reaction was quenched by addition of 40 mL $NaHCO_3$ (sat.). The layers were separated and the aqueous layer was extracted two more times with 20 mL CH_2Cl_2. The combined organic layers were dried over Na_2SO_4 and then evaporated to dryness yielding **L^1OH** as a yellow oil. (2.41 g, 9.9 mmol, 99%). ^{1}H NMR (300 MHz, CD_3CN, RT): δ 2.71 (t, *J* = 6 Hz, 2H, S-C*H*$_2$-C*H*$_2$), 3.56 (t, *J* = 6 Hz, 2H, S-C*H*$_2$-C*H*$_2$), 3.83 (s, 4H, Py-C*H*$_2$-N), 4.0 (br, CH_2-O*H*), 7.17 (m, 2H, Py-*H*$_5$), 7.43 (d, *J* = 8 Hz, 2H, Py-*H*$_3$), 7.66 (td, *J* = 8 Hz, 2 Hz, 2H, Py-*H*$_4$), 8.47 (d, *J* = 5 Hz, 2H, Py-*H*$_6$). ^{13}C NMR (75 MHz, CD_3CN, RT): δ 57.5 (S-*C*H$_2$-*C*H$_2$), 60.3 (S-*C*H$_2$-*C*H$_2$), 61.0 (Py-*C*H$_2$-N), 123.0 (Py-*C*$_3$/Py-*C*$_5$), 123.9 (Py-*C*$_3$/Py-*C*$_5$), 137.4 (Py-*C*$_4$), 149.8 (Py-*C*$_6$), 160.8 (Py-*C*$_2$). ESI-MS found (calculated) for $[M + H]^+$ *m/z* 244.2 (244.1). IR (neat, cm^{-1}): 3270*br*, 2939*w*, 2826*m*, 1592*s*, 1570*m*, 1475*m*, 1433*s*, 1363*m*, 1309*w*, 1249*w*, 1149*m*, 1047*s*, 1002*m*, 758*vs*, 616*s*, 502*m*, 469*m*.

Py_2S

This ligand was synthesized using a modified literature procedure.[27] NaOH (0.30 g, 7.5 mmol) was dissolved in a mixture of 10 mL H_2O and 10 mL ethanol. $Na_2S \cdot 9\ H_2O$ (0.60 g, 2.5 mmol) and 2-(chloromethyl)pyridine hydrochloride (0.82 g, 5.0 mmol) were added. The mixture was refluxed at 95°C for 20 hours and left to cool to RT. The resulting bright orange solution was extracted twice with 20 mL CH_2Cl_2. The organic fractions were combined and dried over Na_2SO_4 to yield **Py_2S** as a yellow oil (0.48 g, 2.2 mmol, 88%). ^{1}H NMR (300 MHz, CD_3OD, RT): δ 3.82 (s, 4H, S-C*H*$_2$-N), 7.25 (dd, *J* = 7 Hz, 5 Hz, 2H, Py-*H*$_5$), 7.42 (d, *J* = 8 Hz, 2H, Py-*H*$_3$), 7.73 (td, *J* = 8 Hz, 2 Hz, 2H, Py-*H*$_4$), 8.42 (d, *J* = 5 Hz, 2H, Py-*H*$_6$). ^{13}C NMR (75 MHz, CD_3OD, RT): δ 38.2 (S-*C*H$_2$-N), 123.5 (Py-*C*$_5$), 124.9 (Py-*C*$_3$), 138.7 (Py-*C*$_4$), 149.7 (Py-*C*$_6$), 159.4 (Py-*C*$_2$). ESI-MS found (calculated) for $[M + H]^+$ *m/z* 217.1 (217.1). IR (neat, cm^{-1}): 3369*br*, 3050*w*, 3008*w*, 2925*w*, 1590*s*, 1568*m*, 1471*m*, 1434*vs*, 1307*w*, 1208*w*, 1151*w*, 1088*w*, 1048*w*, 994*m*, 790*m*, 747*vs*, 711*m*, 627*w*, 579*m*, 484*m*.

5.4 Complex Synthesis

General synthesis procedure

All complexes were synthesized in the same manner unless mentioned otherwise. The ligand was dissolved in methanol, after which $[Cu^{II}(H_2O)_6](BF_4)_2$ and $Cu^{II}Cl_2 \cdot 2\ H_2O$ were added. If there was no formation of powder, diethyl ether was added until precipitation occurred. The powder was filtered and washed with diethyl ether to yield the target complex.

$[Cu^{II}_2(L^1SSL^1)(Cl)_2]_n(BF_4)_{2n}$

From **L^1SSL^1** (67 mg; 0.13 mmol), $[Cu^{II}(H_2O)_6](BF_4)_2$ (46 mg; 0.13 mmol) and $Cu^{II}Cl_2 \cdot 2\ H_2O$ (22 mg; 0.13 mmol), the product $[Cu^{II}_2(\mathbf{L^1SSL^1})(Cl)_2]_n(BF_4)_{2n}$ (104 mg; 0.12 mmol; 90%) was obtained as a blue powder.

Crystals suitable for X-ray structure determination were obtained by slow vapor diffusion of diethyl ether into a CH_3CN solution containing the complex. ESI-MS found (calculated) for $[M - 2\ BF_4]^+$ *m/z* 357.0 (357.0); $[½\ M - Cl - BF_4]^+$ *m/z* 320.9 (321.0); $[½\ M + Cl - BF_4]^+$ *m/z* 392.9 (393.0). IR (neat, cm^{-1}): 1610*m*, 1575*w*, 1486*w*, 1447*m*, 1303*w*, 1286*w*, 1026*vs*, 990*s*, 921*m*, 820*w*, 777*m*, 762*s*, 719*m*, 656*w*, 518*m*, 476*w*, 424*s*. Elemental analysis calcd for $[Cu^{II}_2(\mathbf{L^1SSL^1})(Cl)_2](BF_4)_2 \cdot H_2O$: C 37.11, H 3.78, N 9.27, S 7.07; Found: C 37.40, H 3.96, N 9.25, S 7.23. UV-vis in CH_3CN at 0.1 mM [Cu] concentration: 258 nm (ε = 10 300 $M^{-1}\ cm^{-1}$), 289 nm (ε = 2 700 $M^{-1}\ cm^{-1}$), 680 nm (ε = 190 $M^{-1}\ cm^{-1}$).

$[Cu^{II}_2(\mathbf{L^1{*}SSL^1{*}})(Cl)_2]_n(BF_4)_{2n}$

From $\mathbf{L^1{*}SSL^1{*}}$ (197 mg; 0.36 mmol), $[Cu^{II}(H_2O)_6](BF_4)_2$ (128 mg; 0.36 mmol) and $Cu^{II}Cl_2 \cdot 2\ H_2O$ (62 mg; 0.36 mmol), the product $[Cu^{II}_2(\mathbf{L^1{*}SSL^1{*}})(Cl)_2]_n(BF_4)_{2n}$ (245 mg; 0.27 mmol; 74%) was obtained as a blue powder. ESI-MS found (calculated) for $[M - 2\ BF_4]^{2+}$ *m/z* 371.0 (371.0); $[M + 2\ Cl - 2\ BF_4]^{2+}$ *m/z* 407.0 (406.0); $[½\ M - Cl - BF_4]^+$ *m/z* 335.0 (335.1); $[M - Cu - Cl - 2\ BF_4]^+$ *m/z* 642.3 (642.1). IR (neat, cm^{-1}): 1611*w*, 1574*w*, 1484*w*, 1446*m*, 1284*w*, 1162*w*, 1048*vs*, 1030*vs*, 935*m*, 866*m*, 819*w*, 765*s*, 726*w*, 658*w*, 521*m*, 420*m*. Elemental analysis calcd for $[Cu^{II}_2(\mathbf{L^1{*}SSL^1{*}})(Cl)_2](BF_4)_2$: C 39.32, H 3.96, N 9.17, S 7.00; Found: C 38.69, H 3.99, N 9.19, S 6.88. UV-vis in CH_3CN at 0.1 mM [Cu] concentration: 258 nm (ε = 10 900 $M^{-1}\ cm^{-1}$), 294 nm (ε = 2 900 $M^{-1}\ cm^{-1}$), 690 nm (ε = 210 $M^{-1}\ cm^{-1}$).

$[Cu^{II}_2(\mathbf{L^2SSL^2})(Cl)_2]_n(BF_4)_{2n}$

$\mathbf{L^2SSL^2}$ (72 mg; 0.13 mmol), $[Cu^{II}(H_2O)_6](BF_4)_2$ (46 mg; 0.13 mmol) and $Cu^{II}Cl_2 \cdot 2\ H_2O$ (23 mg; 0.13 mmol) were dissolved in 5 mL CH_3CN. Diethyl ether (13 mL) was added to the bright blue solution. After 15 minutes, the suspension was decanted and filtered. This yielded a bright blue powder that was washed with diethyl ether giving $[Cu^{II}_2(\mathbf{L^2SSL^2})(Cl)_2]_n(BF_4)_{2n}$ (48 mg; 0.05 mmol; 40%). Single crystals suitable for X-ray structure determination were synthesized from $[Cu^{II}(H_2O)_6](ClO_4)_2$ instead of $[Cu^{II}(H_2O)_6](BF_4)_2$. Slow vapor diffusion of diethyl ether into a CH_3CN solution containing the complex, yielded crystals of $[Cu^{II}_2(\mathbf{L^2SSL^2})(Cl)_2]_n(ClO_4)_{2n}$. ESI-MS found (calculated) for $[M - 2\ BF_4]^{2+}$ *m/z* 371.0 (371.0); $[M + 2\ Cl - 2\ BF_4]^{2+}$ *m/z* 406.9 (406.0); $[½\ M - Cl - BF_4]^+$ *m/z* 335.0 (335.1). IR (neat, cm^{-1}): 3554*w*, 1610*m*, 1577*w*, 1447*m*, 1287*w*, 1052*vs*, 1028*vs*, 921*m*, 790*m*, 764*m*, 724*w*, 654*w*, 520*m*, 474*m*. Elemental analysis calcd for $[Cu^{II}_2(\mathbf{L^2SSL^2})(Cl)_2](BF_4)_2$: C 39.32, H 3.96, N 9.17, S 7.00; Found: C 39.23, H 4.01, N 9.12, S 6.96. UV-vis in CH_3CN at 0.1 mM [Cu] concentration: 263 nm (ε = 11 600 $M^{-1}\ cm^{-1}$), 303 nm (ε = 2 800 $M^{-1}\ cm^{-1}$), 720 nm (ε = 270 $M^{-1}\ cm^{-1}$).

$[Cu^{II}_2(\mathbf{L^2{*}SSL^2{*}})(Cl)_2]_n(BF_4)_{2n}$

From $\mathbf{L^2{*}SSL^2{*}}$ (84 mg; 0.15 mmol), $[Cu^{II}(H_2O)_6](BF_4)_2$ (51 mg; 0.15 mmol) and $Cu^{II}Cl_2 \cdot 2\ H_2O$ (25 mg; 0.15 mmol), the product $[Cu^{II}_2(\mathbf{L^2{*}SSL^2{*}})(Cl)_2]_n(BF_4)_{2n}$ (97 mg; 0.10 mmol; 70%) was obtained as a blue powder. ESI-MS found (calculated) for $[M - 2\ BF_4]^{2+}$ *m/z* 386.0 (385.0); $[½\ M - Cl - BF_4]^+$ *m/z* 349.1 (349.1); $[½\ M + Cl - BF_4]^+$ *m/z* 421.0 (421.0); $[M - Cu - Cl - 2\ BF_4]^+$ *m/z* 670.3 (670.2). IR (neat, cm^{-1}): 3565*w*, 2934*w*, 1611*m*, 1576*w*, 1447*m*, 1287*w*, 1052*vs*, 1027*vs*, 867*w*, 771*m*, 729*w*, 654*w*, 521*m*. Elemental analysis calcd for $[Cu^{II}_2(\mathbf{L^2{*}SSL^2{*}})(Cl)_2](BF_4)_2$: C 40.70, H 4.27, N 8.90, S 6.79; Found: C 39.35, H 4.13, N 8.52, S 6.85. UV-vis

in CH_3CN at 0.1 mM [Cu] concentration: 264 nm (ε = 11 400 M^{-1} cm^{-1}), 303 nm (ε = 3 000 M^{-1} cm^{-1}), 730 nm (ε = 270 M^{-1} cm^{-1}).

$[Cu^{II}_2(L^3SSL^3)(Cl)_2]_n(BF_4)_{2n}$

From **L^3SSL^3** (153 mg; 0.27 mmol), $[Cu^{II}(H_2O)_6](BF_4)_2$ (93 mg; 0.27 mmol) and $Cu^{II}Cl_2 \cdot 2\ H_2O$ (46 mg; 0.27 mmol), the product $[Cu^{II}_2(L^3SSL^3)(Cl)_2]_n(BF_4)_{2n}$ (207 mg; 0.22 mmol; 82%) was obtained as a blue powder. ESI-MS found (calculated) for $[½\ M - Cl - BF_4]^+$ *m/z* 349.0 (349.1); $[M - Cu - 2\ Cl - 2\ BF_4]^{2+}$ *m/z* 318.1 (317.6); $[M - Cu - 2\ Cl - 2\ BF_4]^+$ *m/z* 635.3 (635.2). IR (neat, cm^{-1}): 2938*w*, 1612*m*, 1577*w*, 1474*m*, 1459*m*, 1417*w*, 1386*w*, 1349*w*, 1274*w*, 1243*w*, 1172*w*, 1049*vs*, 986*vs*, 923*m*, 852*m*, 805*m*, 722*m*, 519*m*. Elemental analysis calcd for $[Cu^{II}_2(L^3SSL^3)(Cl)_2](BF_4)_2$: C 40.70, H 4.27, N 8.90, S 6.79; Found: C 39.90, H 4.21, N 8.86, S 6.81. UV-vis in CH_3CN at 0.1 mM [Cu] concentration: 265 nm (ε = 13 000 M^{-1} cm^{-1}), 343 nm (ε = 1 600 M^{-1} cm^{-1}), 640 nm (ε = 180 M^{-1} cm^{-1}), 750 nm (ε = 200 M^{-1} cm^{-1}).

$[Cu^{II}_2(L^4SSL^4)(Cl)_2]_n(BF_4)_{2n}$

From **L^4SSL^4** (96 mg; 0.18 mmol), $[Cu^{II}(H_2O)_6](BF_4)_2$ (61 mg; 0.18 mmol) and $Cu^{II}Cl_2 \cdot 2\ H_2O$ (30 mg; 0.18 mmol), the product $[Cu^{II}_2(L^4SSL^4)(Cl)_2]_n(BF_4)_{2n}$ (110 mg; 0.12 mmol; 68%) was obtained as a greyish blue powder. ESI-MS found (calculated) for $[M - 2\ BF_4]^{2+}$ *m/z* 371.0 (371.0); $[M + 2\ Cl - 2\ BF_4]^{2+}$ *m/z* 406.9 (406.0); $[½\ M - Cl - BF_4]^+$ *m/z* 335.0 (335.1); $[M - Cu - Cl - 2\ BF_4]^+$ *m/z* 642.3 (642.1). IR (neat, cm^{-1}): 3628*w*, 1612*m*, 1574*w*, 1487*w*, 1448*m*, 1319*w*, 1300*w*, 1165*w*, 1054*vs*, 1029*vs*, 946*m*, 769*s*, 724*w*, 655*w*, 588*w*, 520*m*, 479*m*. Elemental analysis calcd for $[Cu^{II}_2(L^4SSL^4)(Cl)_2](BF_4)_2 \cdot H_2O$: C 38.56, H 4.10, N 8.99, S 6.86; Found: C 38.45, H 4.36, N 9.12, S 7.03. UV-vis in CH_3CN at 0.1 mM [Cu] concentration: 261 nm (ε = 11 500 M^{-1} cm^{-1}), 293 nm (ε = 3 600 M^{-1} cm^{-1}), 580 nm (ε = 200 M^{-1} cm^{-1}), 670 nm (ε = 180 M^{-1} cm^{-1}).

$[Cu^{II}_2(L^5SSL^5)(Cl)_2]_n(BF_4)_{2n}$

This complex was formed in situ. CH_3CN at 0.1 mM [Cu] concentration: 263 nm (ε = 10 800 M^{-1} cm^{-1}), 292 nm (ε = 3 600 M^{-1} cm^{-1}), 342 nm (ε = 1 900 M^{-1} cm^{-1}), 710 nm (ε = 170 M^{-1} cm^{-1}).

$[Cu^{II}_2(L^1SXSL^1)(Cl)_2]_n(BF_4)_{2n}$

From **L^1SXSL^1** (23 mg; 0.04 mmol), $[Cu^{II}(H_2O)_6](BF_4)_2$ (15 mg; 0.04 mmol) and $Cu^{II}Cl_2 \cdot 2\ H_2O$ (7.4 mg; 0.04 mmol) in CH_3CN, the product $[Cu^{II}_2(L^1SXSL^1)(Cl)_2]_n(BF_4)_{2n}$ (34 mg; 0.04 mmol; 86%) was obtained as a light blue powder. ESI-MS found (calculated) for $[M - 2\ BF_4]^{2+}$ *m/z* 370.0 (370.0). IR (neat, cm^{-1}): 3612*w*, 1611*m*, 1574*w*, 1484*w*, 1447*m*, 1287*w*, 1162*w*, 1054*vs*, 1030*vs*, 901*w*, 852*w*, 819*w*, 765*s*, 728*w*, 656*w*, 521*m*. Elemental analysis calcd for $[Cu^{II}_2(L^1SXSL^1)(Cl)_2](BF_4)_2$: C 39.41, H 3.75, N 9.19, S 7.01; Found: C 38.56, H 3.73, N 9.04, S 6.85. UV-vis in CH_3CN at 0.1 mM [Cu] concentration: 257 nm (ε = 10 800 M^{-1} cm^{-1}), 290 nm (ε = 3 000 M^{-1} cm^{-1}), 700 nm (ε = 190 M^{-1} cm^{-1}).

$[Cu^{II}_2(L^1SL^1)(Cl)_2]_n(BF_4)_{2n}$

From **L^1SL^1** (275 mg; 0.57 mmol), $[Cu^{II}(H_2O)_6](BF_4)_2$ (196 mg; 0.57 mmol) and $Cu^{II}Cl_2 \cdot 2\ H_2O$ (97 mg; 0.57 mmol), the product $[Cu^{II}_2(L^1SL^1)(Cl)_2]_n(BF_4)_{2n}$ (370 mg; 0.43 mmol; 76%) was obtained as a light blue powder.

Crystals suitable for X-ray structure determination were obtained by slow vapor diffusion of diethyl ether into a CH_3CN solution containing the complex. ESI-MS found (calculated) for $[M - 2\ BF_4]^{2+}$ *m/z* 341.0 (341.0). IR (neat, cm^{-1}): 3612*w*, 1611*m*, 1574*w*, 1481*w*, 1444*m*, 1290*w*, 1088*m*, 1049*vs*, 1030*vs*, 995*m*, 973*w*, 946*w*, 906*w*, 819*w*, 777*m*, 761*m*, 717*m*, 654*w*, 521*w*. Elemental analysis calcd for $[Cu^{II}_2(\mathbf{L^1SL^1})(Cl)_2](BF_4)_2$: C 39.28, H 3.77, N 9.81, S 3.74; Found: C 40.13, H 3.85, N 10.15, S 3.67. UV-vis in CH_3CN at 0.1 mM [Cu] concentration: 256 nm (ε = 10 600 M^{-1} cm^{-1}), 290 nm (ε = 2 900 M^{-1} cm^{-1}), 690 nm (ε = 110 M^{-1} cm^{-1}).

$[Cu^{II}_2(\mathbf{L^1C_6L^1})(Cl)_2]_n(BF_4)_{2n}$

From $\mathbf{L^1C_6L^1}$ (102 mg; 0.21 mmol), $[Cu^{II}(H_2O)_6](BF_4)_2$ (74 mg; 0.21 mmol) and $Cu^{II}Cl_2 \cdot 2\ H_2O$ (36 mg; 0.21 mmol), the product $[Cu^{II}_2(\mathbf{L^1C_6L^1})(Cl)_2]_n(BF_4)_{2n}$ (158 mg; 0.19 mmol; 87%) was obtained as a dark blue powder. Crystals suitable for X-ray structure determination were obtained by slow vapor diffusion of di-isopropyl ether into a CH_3CN solution containing the complex. ESI-MS found (calculated) for $[M - 2\ BF_4]^{2+}$ *m/z* 339.1 (339.1). IR (neat, cm^{-1}): 3090*w*, 2933*w*, 2853*w*, 1612*m*, 1574*w*, 1484*w*, 1446*m*, 1283*m*, 1088*m*, 1049*vs*, 1031*vs*, 897*m*, 883*m*, 817*w*, 766*s*, 726*w*, 660*w*, 521*m*, 492*w*. Elemental analysis calcd for $[Cu^{II}_2(\mathbf{L^1C_6L^1})(Cl)_2](BF_4)_2$: C 42.28, H 4.26, N 9.86; Found: C 42.49, H 4.35, N 9.93. UV-vis in CH_3CN at 0.1 mM [Cu] concentration: 256 nm (ε = 11 800 M^{-1} cm^{-1}), 291 nm (ε = 3 000 M^{-1} cm^{-1}), 660 nm (ε = 140 M^{-1} cm^{-1}).

$[Cu^{II}_2(\mathbf{L^1PhL^1})(Cl)_2]_n(BF_4)_{2n}$

From $\mathbf{L^1PhL^1}$ (166 mg; 0.35 mmol), $[Cu^{II}(H_2O)_6](BF_4)_2$ (121 mg; 0.35 mmol) and $Cu^{II}Cl_2 \cdot 2\ H_2O$ (60 mg; 0.35 mmol), the product $[Cu^{II}_2(\mathbf{L^1PhL^1})(Cl)_2]_n(BF_4)_{2n}$ (249 mg; 0.30 mmol; 84%) was obtained as a green powder. ESI-MS found (calculated) for $[M - 2\ BF_4]^{2+}$ *m/z* 335.0 (335.0); $[M - Cu - Cl - 2\ BF_4]^{+}$ *m/z* 570.2 (570.1). IR (neat, cm^{-1}): 2972*w*, 1611*m*, 1575*w*, 1486*w*, 1449*m*, 1288*m*, 1052*vs*, 1031*vs*, 870*m*, 769*s*, 698*m*, 657*m*, 538*w*, 521*m*. Elemental analysis calcd for $[Cu^{II}_2(\mathbf{L^1PhL^1})(Cl)_2](BF_4)_2 \cdot 2\ CH_3CN$: C 44.09, H 3.70, N 12.10; Found: C 43.18, H 3.82, N 11.80. UV-vis in CH_3CN at 0.1 mM [Cu] concentration: 260 nm (ε = 11 500 M^{-1} cm^{-1}), 310 nm (ε = 2 000 M^{-1} cm^{-1}), 380 nm (ε = 410 M^{-1} cm^{-1}), 700 nm (ε = 150 M^{-1} cm^{-1}).

$[Cu^{II}(\mathbf{Py_3N})(Cl)](BF_4)$

From $\mathbf{Py_3N}$ (160 mg; 0.55 mmol), $[Cu^{II}(H_2O)_6](BF_4)_2$ (96 mg; 0.28 mmol) and $Cu^{II}Cl_2 \cdot 2\ H_2O$ (47 mg; 0.28 mmol), the product $[Cu^{II}(\mathbf{Py_3N})(Cl)](BF_4)$ (251 mg; 0.53 mmol; 96%) was obtained as a mint green powder. ESI-MS found (calculated) for $[M - BF_4]^{+}$ *m/z* 388.0 (388.1). IR (neat, cm^{-1}): 2974*w*, 1607*m*, 1575*w*, 1480*w*, 1438*m*, 1307*w*, 1263*w*, 1159*w*, 1113*w*, 1090*m*, 1047*vs*, 1021*s*, 958*m*, 841*w*, 771*m*, 761*s*, 643*w*, 506*m*. Elemental analysis calcd for $[Cu^{II}(\mathbf{Py_3N})(Cl)](BF_4)$: C 43.75, H 4.08, N 11.34; Found: C 44.88, H 4.40, N 11.59. UV-vis in CH_3CN at 0.1 mM [Cu] concentration: 230 nm (ε = 7 600 M^{-1} cm^{-1}), 261 nm (ε = 12 100 M^{-1} cm^{-1}), 299 nm (ε = 3 100 M^{-1} cm^{-1}), 730 nm (ε = 90 M^{-1} cm^{-1}), 940 nm (ε = 200 M^{-1} cm^{-1}).

$[Cu^{II}(\mathbf{L^1SCH_3})(Cl)](BF_4)$

From $\mathbf{L^1SCH_3}$ (94 mg; 0.34 mmol), $[Cu^{II}(H_2O)_6](BF_4)_2$ (59 mg; 0.17 mmol) and $Cu^{II}Cl_2 \cdot 2\ H_2O$ (29 mg; 0.17 mmol), the product $[Cu^{II}(\mathbf{L^1SCH_3})(Cl)](BF_4)$ (110 mg; 0.24 mmol; 70%) was obtained as a dark blue crystalline solid. Crystals suitable for X-ray structure determination were obtained by slow vapor diffusion of diethyl ether

into a methanol solution containing the complex. ESI-MS found (calculated) for $[M - BF_4]^+$ *m/z* 370.9 (371.0). IR (neat, cm^{-1}): 1611*m*, 1441*m*, 1284*m*, 1046*vs*, 1029*vs*, 1002*m*, 907*m*, 783*m*, 759*m*, 519*m*. Elemental analysis calcd for $[Cu^{II}(\mathbf{L^1SCH_3})(Cl)](BF_4)$: C 39.23, H 4.17, N 9.15, S 6.98; Found: C 39.73, H 4.44, N 9.25, S 7.05. UV-vis in acetonitrile at 0.1 mM [Cu] concentration: 258 nm (ε = 10 800 M^{-1} cm^{-1}), 297 nm (ε = 3 400 M^{-1} cm^{-1}), 700 nm (ε = 130 M^{-1} cm^{-1}), 890 nm (ε = 170 M^{-1} cm^{-1}).

$[Cu^{II}(\mathbf{L^1{*}SCH_3})(Cl)](BF_4)$

From $\mathbf{L^1{*}SCH_3}$ (178 mg; 0.62 mmol), $[Cu^{II}(H_2O)_6](BF_4)_2$ (107 mg; 0.31 mmol) and $Cu^{II}Cl_2 \cdot 2\ H_2O$ (53 mg; 0.31 mmol), the product $[Cu^{II}(\mathbf{L^1{*}SCH_3})(Cl)](BF_4)$ (157 mg; 0.33 mmol; 54%) was obtained as a blue powder. Crystals suitable for X-ray structure determination were obtained by slow vapor diffusion of diethyl ether into a methanol solution containing the complex. ESI-MS found (calculated) for $[M - BF_4]^+$ *m/z* 385.0 (385.0). IR (neat, cm^{-1}): 1609*m*, 1573*w*, 1483*w*, 1444*m*, 1302*w*, 1285*w*, 1160*w*, 1054*vs*, 1028*vs*, 863*w*, 820*w*, 766*s*, 652*w*, 520*m*. Elemental analysis calcd for $[Cu^{II}(\mathbf{L^1{*}SCH_3})(Cl)](BF_4)$: C 40.61, H 4.47, N 8.88, S 6.78; Found: C 40.17, H 4.51, N 8.68, S 7.03. UV-vis in CH_3CN at 0.1 mM [Cu] concentration: 257 nm (ε = 11 000 M^{-1} cm^{-1}), 299 nm (ε = 3 600 M^{-1} cm^{-1}), 690 nm (ε = 130 M^{-1} cm^{-1}), 880 nm (ε = 160 M^{-1} cm^{-1}).

$[Cu^{II}(\mathbf{L^2SCH_3})(Cl)](BF_4)$

From $\mathbf{L^2SCH_3}$ (116 mg; 0.40 mmol), $[Cu^{II}(H_2O)_6](BF_4)_2$ (70 mg; 0.20 mmol) and $Cu^{II}Cl_2 \cdot 2\ H_2O$ (35 mg; 0.20 mmol), the product $[Cu^{II}(\mathbf{L^2SCH_3})(Cl)](BF_4)$ (96 mg; 0.20 mmol; 50%) was obtained as a blue powder. Crystals suitable for X-ray structure determination were obtained by slow vapor diffusion of diethyl ether into a methanol solution containing the complex. ESI-MS found (calculated) for $[M - BF_4]^+$ *m/z* 385.0 (385.0); $[M - Cl - BF_4]^+$ *m/z* 350.0 (350.1). IR (neat, cm^{-1}): 2932*w*, 1610*m*, 1578*w*, 1460*w*, 1445*m*, 1287*w*, 1175*w*, 1050*vs*, 1026*vs*, 961*m*, 911*m*, 791*m*, 764*m*, 725*w*, 654*w*, 520*m*. Elemental analysis calcd for $[Cu^{II}(\mathbf{L^2SCH_3})(Cl)](BF_4)$: C 40.61, H 4.47, N 8.88, S 6.78; Found: C 40.64, H 4.59, N 8.78, S 6.71. UV-vis in CH_3CN at 0.1 mM [Cu] concentration: 265 nm (ε = 10 300 M^{-1} cm^{-1}), 305 nm (ε = 3 600 M^{-1} cm^{-1}), 350 nm (ε = 2 300 M^{-1} cm^{-1}), 690 nm (ε = 320 M^{-1} cm^{-1}), 870 nm (ε = 310 M^{-1} cm^{-1}).

$[Cu^{II}(\mathbf{L^3SCH_3})(Cl)](BF_4)$

From $\mathbf{L^3SCH_3}$ (154 mg; 0.51 mmol), $[Cu^{II}(H_2O)_6](BF_4)_2$ (88 mg; 0.26 mmol) and $Cu^{II}Cl_2 \cdot 2\ H_2O$ (44 mg; 0.26 mmol), the product $[Cu^{II}(\mathbf{L^3SCH_3})(Cl)](BF_4)$ (195 mg; 0.40 mmol; 78%) was obtained as a dark blue powder. Crystals suitable for X-ray structure determination were obtained by slow vapor diffusion of diethyl ether into a methanol solution containing the complex. ESI-MS found (calculated) for $[M - BF_4]^+$ *m/z* 399.0 (399.1); $[M - Cl - BF_4]^+$ *m/z* 364.0 (364.1). IR (neat, cm^{-1}): 2929*w*, 1610*m*, 1576*w*, 1474*m*, 1457*m*, 1432*w*, 1349*w*, 1287*w*, 1241*w*, 1094*m*, 1049*vs*, 1027*vs*, 964*m*, 915*w*, 803*s*, 792*m*, 773*m*, 648*w*, 520*m*. Elemental analysis calcd for $[Cu^{II}(\mathbf{L^3SCH_3})(Cl)](BF_4)$: C 41.90, H 4.76, N 8.62, S 6.58; Found: C 42.08, H 4.73, N 8.69, S 6.52. UV-vis in CH_3CN at 0.1 mM [Cu] concentration: 267 nm (ε = 11 700 M^{-1} cm^{-1}), 319 nm (ε = 2 600 M^{-1} cm^{-1}), 358 nm (ε = 2 400 M^{-1} cm^{-1}), 650 nm (ε = 300 M^{-1} cm^{-1}), 840 nm (ε = 160 M^{-1} cm^{-1}).

*[Cu^{II}(**L^1OH**)(Cl)](BF_4)*

From **L^1OH** (194 mg; 0.80 mmol), [$Cu^{II}(H_2O)_6$](BF_4)$_2$ (138 mg; 0.40 mmol) and $Cu^{II}Cl_2 \cdot 2\ H_2O$ (68 mg; 0.40 mmol), the product [Cu^{II}(**L^1OH**)(Cl)](BF_4) (307 mg; 0.72 mmol; 90%) was obtained as a blue powder. ESI-MS found (calculated) for [M – BF_4]$^+$ *m/z* 341.0 (341.0). IR (neat, cm^{-1}): 3474*br*, 2949*w*, 1611*m*, 1575*w*, 1480*w*, 1443*m*, 1287*m*, 1060*vs*, 1031*vs*, 1005*s*, 983*s*, 955*m*, 871*m*, 798*s*, 763*vs*, 723*m*, 655*m*, 519*m*, 483*m*. Elemental analysis calcd for [Cu^{II}(**L^1OH**)(Cl)](BF_4): C 39.49, H 3.99, N 9.79; Found: C 39.13, H 3.97, N 9.73. UV-vis in CH_3CN at 0.1 mM [Cu] concentration: 256 nm (ε = 11 300 M^{-1} cm^{-1}), 285 nm (ε = 3 400 M^{-1} cm^{-1}), 690 nm (ε = 90 M^{-1} cm^{-1}).

*[Cu^{II}(**L^1NH_2**)(Cl)](BF_4)*

L^1NH_2 (133 mg; 0.55 mmol), [$Cu^{II}(H_2O)_6$](BF_4)$_2$ (95 mg; 0.27 mmol) and $Cu^{II}Cl_2 \cdot 2\ H_2O$ (47 mg; 0.27 mmol) were dissolved in 10 mL CH_3CN. This solution was added drop wise to 100 mL diethyl ether. The powder was filtered and washed with diethyl ether yielding [Cu^{II}(**L^1NH_2**)(Cl)](BF_4) (141 mg; 0.33 mmol; 60%) as a light blue powder. Crystals suitable for X-ray structure determination were obtained by slow vapor diffusion of diethyl ether into a CH_3CN solution containing the complex. ESI-MS found (calculated) for [M – BF_4]$^+$ *m/z* 340.1 (340.1). IR (neat, cm^{-1}): 3366*m*, 3303*w*, 1605*m*, 1575*w*, 1477*w*, 1447*m*, 1439*m*, 1265*w*, 1045*vs*, 1021*vs*, 964*s*, 941*m*, 886*w*, 765*vs*, 643*m*, 566*m*, 522*m*, 490*m*. Elemental analysis calcd for [Cu^{II}(**L^1NH_2**)(Cl)](BF_4): C 39.28, H 4.24, N 13.09; Found: C 39.34, H 4.27, N 12.97. UV-vis in CH_3CN at 0.1 mM [Cu] concentration: 258 nm (ε = 9 800 M^{-1} cm^{-1}), 293 nm (ε = 3 900 M^{-1} cm^{-1}), 700 nm (ε = 110 M^{-1} cm^{-1}), 690 nm (ε = 220 M^{-1} cm^{-1}).

*[Cu^{II}(**Py_2NH**)(Cl)](BF_4)*

From **Py_2NH** (223 mg; 1.12 mmol), [$Cu^{II}(H_2O)_6$](BF_4)$_2$ (193 mg; 0.56 mmol) and $Cu^{II}Cl_2 \cdot 2\ H_2O$ (96 mg; 0.56 mmol), the product [Cu^{II}(**Py_2NH**)(Cl)](BF_4) (341 mg; 0.89 mmol; 79%) was obtained as a dark blue powder. ESI-MS found (calculated) for [M – BF_4]$^+$ *m/z* 296.9 (297.0). IR (neat, cm^{-1}): 3466*w*, 3215*w*, 1611*m*, 1574*w*, 1483*w*, 1445*m*, 1285*w*, 1051*vs*, 1028*vs*, 1001*vs*, 935*s*, 815*w*, 764*vs*, 727*m*, 656*w*, 520*m*, 483*w*. Elemental analysis calcd for [Cu^{II}(**Py_2NH**)(Cl)](BF_4) · H_2O: C 35.76, H 3.75, N 10.43; Found: C 37.01, H 3.85, N 10.68. UV-vis in CH_3CN at 0.1 mM [Cu] concentration: 255 nm (ε = 12 000 M^{-1} cm^{-1}), 293 nm (ε = 2 100 M^{-1} cm^{-1}), 660 nm (ε = 120 M^{-1} cm^{-1}).

*[Cu^{II}(**Py_2S**)(Cl)](BF_4)*

From **Py_2S** (112 mg; 0.52 mmol), [$Cu^{II}(H_2O)_6$](BF_4)$_2$ (89 mg; 0.26 mmol) and $Cu^{II}Cl_2 \cdot 2\ H_2O$ (44 mg; 0.26 mmol), the product [Cu^{II}(**Py_2S**)(Cl)](BF_4) (159 mg; 0.40 mmol; 76%) was obtained as a turquoise blue powder. ESI-MS found (calculated) for [M – BF_4]$^+$ *m/z* 313.9 (314.0); [M + CH_3CN – Cl – BF_4]$^+$ *m/z* 320.0 (320.0). IR (neat, cm^{-1}): 2929*w*, 1602*m*, 1568*w*, 1474*m*, 1446*m*, 1406*m*, 1262*m*, 1106*m*, 1074*s*, 1052*s*, 1024*s*, 997*vs*, 890*m*, 783*vs*, 764*m*, 717*m*, 649*m*, 518*m*, 475*m*. Elemental analysis calcd for [Cu^{II}(**Py_2S**)(Cl)](BF_4): C 35.84, H 3.01, N 6.97, S 7.97; Found: C 34.85, H 2.89, N 6.65, S 8.06. UV-vis in CH_3CN at 0.1 mM [Cu] concentration: 265 nm (ε = 11 600 M^{-1} cm^{-1}), 320 nm (ε = 1 900 M^{-1} cm^{-1}), 360 nm (ε = 2 800 M^{-1} cm^{-1}), 690 nm (ε = 220 M^{-1} cm^{-1}).

5.5 Catalysis Experiments

To 1 000 µL CH_3CN in a 1 cm quartz cuvette was added 1 000 µL catalyst solution (1.2 mM mononuclear complex or 0.6 mM dinuclear complex solutions in 25 mL CH_3CN; when the complex was made in situ Na_2SO_4 was added to the stock solution to remove most of the H_2O present), followed by 1 000 µL 3,5-di-*tert*-butylcatechol solution (60 mM stock solution in 25 mL CH_3CN). The solution was stirred and temperature-controlled (temperature was kept at 25 °C) using a Cary Single Cell Peltier Accessory from Agilent Technologies (Type SPV-1X0) and a mixture of N_2:O_2(50:50) was bubbled through the solution with a needle. At the start of the measurement NEt_3 (8.36 µL, 0.06 mmol) was added and the formation of 3,5-di-*tert*-butyl-*o*-benzoquinone was monitored by measuring the absorbance at 400 nm every 0.1 sec. The resulting solution contains concentrations of 0.4 mM [Cu], 20 mM 3,5-DTBC and 20 mM NEt_3 unless mentioned otherwise. Every reaction was carried out at least four or five times; the error of the reaction is ≤ 8%. The average values are reported.

Acknowledgements

This research has been financially supported by the National Research School Combination NRSC-Catalysis, a joint activity of the graduate research schools NIOK, HRSMC, and EPL. We thank John van Dijk for ESI-MS analysis, Fons Lefeber and Karthick Sai Sankar Gupta for assistance with the NMR experiments, and Jos van Brussel for elemental analysis. We thank undergraduate students Mart van Meurs, Suzanne van Daal and Mickey Harvey for the synthesis of $[Cu^{II}_2(\mathbf{L^1C_6L^1})(Cl)_2]n(BF_4)_{2n}$, $[Cu^{II}(\mathbf{L^1NH_2})(Cl)](BF_4)$ and $\mathbf{Py_2S}$.

References

1. N. D. J. Branscombe, A. J. Blake, A. MarinBecerra, W. S. Li, S. Parsons, L. RuizRamirez and M. Schroder, *Chem. Commun.*, 1996, 2573-2574.
2. W. Rammal, C. Belle, C. Beguin, C. Duboc, C. Philouze, J.-L. Pierre, L. Le Pape, S. Bertaina, E. Saint-Aman and S. Torelli, *Inorg. Chem.*, 2006, **45**, 10355-10362.
3. R. P. Houser, J. A. Halfen, V. G. Young, N. J. Blackburn and W. B. Tolman, *J. Am. Chem. Soc.*, 1995, **117**, 10745-10746.
4. E. C. M. Ording-Wenker, M. van der Plas, M. A. Siegler, C. Fonseca Guerra and E. Bouwman, *Chem. Eur. J.*, 2014, **20**, 16913-16921.
5. Y. Ueno, Y. Tachi and S. Itoh, *J. Am. Chem. Soc.*, 2002, **124**, 12428-12429.
6. A. Neuba, R. Haase, W. Meyer-Klaucke, U. Flörke and G. Henkel, *Angew. Chem. Int. Ed.*, 2012, **51**, 1714-1718.
7. S. Itoh, M. Nagagawa and S. Fukuzumi, *J. Am. Chem. Soc.*, 2001, **123**, 4087-4088.
8. E. C. M. Ording-Wenker, M. van der Plas, M. A. Siegler, S. Bonnet, F. M. Bickelhaupt, C. Fonseca Guerra and E. Bouwman, *Inorg. Chem.*, 2014, **53**, 8494-8504.
9. R. R. Jacobson, Z. Tyeklar, A. Farooq, K. D. Karlin, S. Liu and J. Zubieta, *J. Am. Chem. Soc.*, 1988, **110**, 3690-3692.

10. H. Hayashi, S. Fujinami, S. Nagatomo, S. Ogo, M. Suzuki, A. Uehara, Y. Watanabe and T. Kitagawa, *J. Am. Chem. Soc.*, 2000, **122**, 2124-2125.
11. J. A. Halfen, S. Mahapatra, E. C. Wilkinson, S. Kaderli, V. G. Young, L. Que, A. D. Zuberbuhler and W. B. Tolman, *Science*, 1996, **271**, 1397-1400.
12. W. B. Tolman, *Acc. Chem. Res.*, 1997, **30**, 227-237.
13. M. T. Kieber-Emmons, J. W. Ginsbach, P. K. Wick, H. R. Lucas, M. E. Helton, B. Lucchese, M. Suzuki, A. D. Zuberbühler, K. D. Karlin and E. I. Solomon, *Angew. Chem. Int. Ed.*, 2014, **53**, 4935-4939.
14. I. A. Koval, P. Gamez, C. Belle, K. Selmeczi and J. Reedijk, *Chem. Soc. Rev.*, 2006, **35**, 814-840.
15. C. Eicken, B. Krebs and J. C. Sacchettini, *Curr. Opin. Struc. Biol.*, 1999, **9**, 677-683.
16. S. E. Allen, R. R. Walvoord, R. Padilla-Salinas and M. C. Kozlowski, *Chem. Rev.*, 2013, **113**, 6234-6458.
17. E. Monzani, L. Quinti, A. Perotti, L. Casella, M. Gullotti, L. Randaccio, S. Geremia, G. Nardin, P. Faleschini and G. Tabbi, *Inorg. Chem.*, 1998, **37**, 553-562.
18. J. Reedijk, *Science*, 2005, **308**, 1876-1877.
19. E. C. M. Ording-Wenker, M. A. Siegler, M. Lutz and E. Bouwman, *Inorg. Chem.*, 2013, **52**, 13113-13122.
20. H. Ertuerk, A. Hofmann, R. Puchta and R. van Eldik, *Dalton Trans.*, 2007, 2295-2301.
21. S. Turba, O. Walter, S. Schindler, L. P. Nielsen, A. Hazell, C. J. McKenzie, F. Lloret, J. Cano and M. Julve, *Inorg. Chem.*, 2008, **47**, 9612-9623.
22. S. Schindler, D. J. Szalda and C. Creutz, *Inorg. Chem.*, 1992, **31**, 2255-2264.
23. G. J. P. Britovsek, J. England and A. J. P. White, *Inorg. Chem.*, 2005, **44**, 8125-8134.
24. E. C. M. Ording-Wenker, M. A. Siegler and E. Bouwman, *Inorg. Chim. Acta*, 2015, **428**, 193-202.
25. E. A. Ambundo, M. V. Deydier, A. J. Grall, N. Aguera-Vega, L. T. Dressel, T. H. Cooper, M. J. Heeg, L. A. Ochrymowycz and D. B. Rorabacher, *Inorg. Chem.*, 1999, **38**, 4233-4242.
26. K. Sundaravel, M. Sankaralingam, E. Suresh and M. Palaniandavar, *Dalton Trans.*, 2011, **40**, 8444-8458.
27. H. J. J. B. Martel and M. Rasmussen, *Tetrahedron Lett.*, 1971, **12**, 3843-3846.
28. R. Herges, A. Dikmans, U. Jana, F. Kohler, P. G. Jones, I. Dix, T. Fricke and B. Konig, *Eur. J. Org. Chem.*, 2002, 3004-3014.
29. E. C. M. Tse, D. Schilter, D. L. Gray, T. B. Rauchfuss and A. A. Gewirth, *Inorg. Chem.*, 2014, **53**, 8505-8516.
30. A. W. Addison, T. N. Rao, J. Reedijk, J. Vanrijn and G. C. Verschoor, *J. Chem. Soc., Dalton Trans.*, 1984, 1349-1356.

31. M. Schatz, M. Leibold, S. P. Foxon, M. Weitzer, F. W. Heinemann, F. Hampel, O. Walter and S. Schindler, *Dalton Trans.*, 2003, 1480-1487.
32. A. Winter, A. Zabel and P. Strauch, *Int. J. Mol. Sci.*, 2012, **13**, 1612-1619.
33. E. I. Solomon, M. J. Baldwin and M. D. Lowery, *Chem. Rev.*, 1992, **92**, 521-542.
34. O. V. Kovalchukova, K. K. Palkina, S. B. Strashnova and B. E. Zaitsev, *Russ. J. Coord. Chem.*, 2008, **34**, 830-835.
35. A. M. Thomas, B.-L. Lin, E. C. Wasinger and T. D. P. Stack, *J. Am. Chem. Soc.*, 2013, **135**, 18912-18919.
36. A. C. D. Midoes, P. E. Aranha, M. P. dos Santos, E. Tozzo, S. Romera, R. H. d. A. Santos and E. R. Dockal, *Polyhedron*, 2008, **27**, 59-64.
37. K. Selmeczi, M. Reglier, M. Giorgi and G. Speier, *Coord. Chem. Rev.*, 2003, **245**, 191-201.
38. T. Osako, Y. Ueno, Y. Tachi and S. Itoh, *Inorg. Chem.*, 2004, **43**, 6516-6518.
39. G. M. Sheldrick, *Acta Crystallogr. Sect. A*, 2008, **64**, 112-122.
40. A. J. M. Duisenberg, R. W. W. Hooft, A. M. M. Schreurs and J. Kroon, *J. Appl. Crystallogr.*, 2000, **33**, 893-898.
41. G. M. Sheldrick, Universität Göttingen, Germany, 1999.
42. R. Herbst-Irmer and G. M. Sheldrick, *Acta Crystallogr. Sect. B: Struct. Sci.*, 1998, **54**, 443-449.
43. A. L. Spek, *Acta Crystallogr. Sect. D. Biol. Crystallogr.*, 2009, **65**, 148-155.

Table of Contents Entry

High activity for the catalytic oxidation of 3,5-di-tert-butylcatechol was achieved with complexes of ligands that stabilize the biomimetic Cu^{II} μ-thiolate complex, hinting at a similarity with the required Cu-oxo intermediates.